Chapter

Interaction of Magnetic Fields on Ferrofluidic Taylor-Couette Flow

Sebastian Altmeyer

Abstract

When studying ferrofluidic flows, as one example of magnetic flow dynamics, in terms of instability, bifurcation, and properties, one quickly finds out the additional challenges magnetic fluids introduce compared to the investigation of "*classical*", "*ordinary*" shear flows without any kind of particles. Approximation of ferrofluids as fluids including point-size particles or, more realistic fine size particles, the relaxation times of the magnetic particle, their interaction between each other, i.e., the agglomeration and chain forming effects, and the interaction/response between any external applied field and the internal magnetization are just few examples of challenges to overcome. Further dependence on the considered model system, the direction of the external applied magnetic field (homogeneous or inhomogeneous) is crucial, as it can break the system symmetry and thus generate new solutions. As a result, the classical Navier–Stokes equations become modified to the more complex ferrohydrodynamical equation of motion, incorporating magnetic field and magnetization of the fluid itself, which typically makes numerical simulations expensive and challenging. This chapter provides an overview of the tasks/difficulties from describing and simulating magnetic particles, their interaction, and thus finally resulting modification in rotating flow structures and in particular instabilities and bifurcation behavior.

Keywords: magnetic fluid, complex system, ferrofluid, instabilities, bifurcation, symmetry-breaking, vortex, growth rate, finite-size effect, internal magnetic field, particle interaction, agglomeration, elongational flow

1. Introduction

Ferrofluids [1] represent one example of magnetic particles with a variety of applications, ranging from liquid seals in rotating systems, their use in computer hard drives, as well as in laboratory experiments, to study geophysical flows [2, 3]. However, deeper fundamental study of their magnetohydrodynamics is inevitable, as there are many modeling assumptions that have been implemented to make theoretical descriptions tractable. Ferrofluids are manufactured fluids which consist of dispersions of magnetized nanoparticles in various kinds of liquid carriers. Stabilizing against agglomeration is typically achieved by the addition of a surfactant monolayer onto the magnetic particles. Being no magnetic field present, the magnetic nanoparticles are randomly orientated, which results in a zero-net magnetization of the fluid. Only effect of the present nanoparticles is a typically small alteration to the fluid's density and viscosity. Applying a sufficiently strong

magnetic field, the ferrofluid flows toward certain regions of the magnetic field. The hydrodynamics of the system can be significantly changed, and properties of the fluid, e.g., the viscosity, are altered. Therefore, nowadays, they are widely used by various car manufactures in order to provide adaptable suspensions, i.e., changing the damping characteristics of an antishock/damper due to modified viscosity of the ferrofluid under influence of an external applied magnetic field. Both numerical simulations and experiments show that any applied magnetic field, whether radial, axial, azimuthal, transversal, or any combination of the previous stabilizes the basic state [4–9]. This stabilization effect depends, among others, on the particle-particle interactions of the fluid [9]. A strong interaction leads to large/crucial changes in flow behavior, which are driven by the formation of internal flow structures. While an axisymmetric field leaves the flow structures untouched (compared to classical Couette flow), a finite transverse, in-plane magnetic-field component breaks axisymmetry, enforcing new nonlinear effects, modify present flow structures, and can produce new flow structures.

Among various others, one important point to look at is the applied magnetic field, in particular its characteristics while penetrating a moving ferrofluid. In order to describe the hydrodynamics of ferrofluids in containers/boxes typically, models are used which assume that the internal magnetic field and the external applied magnetic field are equal [4–6]. However, such a simplification is only a leading order approximation, as the magnetic field in the container typically is *modified, b*ased on the magnetic susceptibility of the ferrofluid. First work trying to account for modifications [15] includes an expression for the angular velocity of the ferrofluid particles, which differs from the ferrofluid itself due to the magnetic torques acting on the particles. The results are significant *differences* from the external field, providing among others, a much changed body force in the governing equations. More concretely, the interaction between a uniform external field and the susceptibility of the ferrofluid-filled annulus can be shown to result in a field with an $1/r^2$ radial dependence superimposed on the external field.

Further common assumption when describing the hydrodynamics of magnetic particles as ferrofluids is to consider them as point-wise objects and ignore their finite size and specific properties. However, in real, such particles typically aggregate to form clusters having the form of chains, and thus they hinder the free flow of the fluid and increase the viscosity [9–11], and change their rheology and transport properties [14]. In this type of structure's formation, it is also assumed that the interaction parameter is usually greater than unity [1], and thus the strength of the grain-grain interaction can be measured in terms of the total momentum of a particle. Regarding the magneto-dissipative structure of ferrofluid dynamics, one can derive, based on general principles, an equation for macroscopic ferrofluid dynamics. The magnetization's relaxation equation includes an additional term that is proportional to the product of the magnetization's magnitude and the symmetric part of the velocity gradient tensor, which can describe an *elongational flow* scaled by a so-called *transport coefficient* λ_2. Such description also exists in the dynamics of nematic liquid crystals, as the flow alignment modifies the director field in an applied shear flow [16].

It is worth to mention that there are further crucial and important considerations for describing ferrofluids and in general fluids with magnetic particles which are also important as the discussed ones. However, these are not considered in the present chapter. Therefore, we refer to the huge amount of literature, which can be essentially found by the presented references. Two prominent examples of these further considerations are the modulation of the relaxation times of magnetic particles [7, 13], e.g., Neel's or Braun's and the consideration of monodisperse vs. polydisperse materials [7, 17, 18].

In this chapter, we will consider a rotating ferrofluid in Taylor-Couette geometry. First, we are going to describe the modifications in flow solutions and its structural properties and alterations in primary supercritical bifurcation thresholds induced/forced by an external applied magnetic field. Following, we will discuss two different approaches to come to a more realistic description of ferrofluidic flows. Therefore, we will modify and extend the basic ferrohydrodynamical equations. First, considering a modification of the internal magnetic field, which differs from the external applied one due to its internal magnetization. Second incorporating elongational flow. The latter aims to consider finite size effects of the magnetic particles, as well as agglomeration and chain formation procedures.

2. System and theoretical description

As a prototypical system to investigate the influences of a magnetic field on a rotating ferrofluid system, we consider Taylor-Couette flow (Taylor Couette system, TCS) [19, 20] driven by the independent differential rotation of two concentric cylinders (**Figure 1**).

The inner cylinder of radius r_1 rotates at ω_1, and the outer cylinder of radius r_2 rotates at ω_2. If not other stated, in this chapter, periodic boundary conditions are considered in the axial direction with periodicity of length λ and no-slip boundary conditions on the cylinder walls. The system is described using a cylindrical polar coordinate system (r, θ, z) with a velocity field $\vec{u} = (u, v, w)$. The radius ratio of the cylinders is $\beta = r_1/r_2$, and the aspect ratio is $\Gamma = \lambda/(r_2 - r_1)$. The gap between the cylinders is filled with a viscous, incompressible, and isothermal ferrofluid. An external homogeneous magnetic field $\vec{H}_{ext} = H_x \vec{e}_x + H_z \vec{e}_z$ is applied, where $x = r\cos\theta$ is the transverse direction and z is the axial direction, respectively (**Figure 1**).

The flow dynamics of an incompressible homogeneous monodisperse ferrofluid with kinematic viscosity ν and density ρ is governed by the incompressible Navier–Stokes equations, including magnetic terms and the continuity equation. Following, an approach based on the model of Niklas [4, 5] is used, where the magnetic fluid is

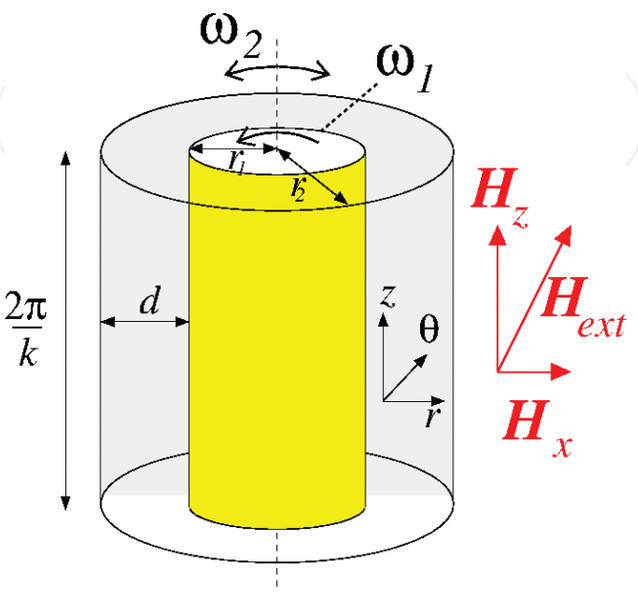

Figure 1
Schematic of the Taylor-Couette system with an external applied homogeneous magnetic field $\vec{H}_{ext} = H_x \vec{e}_x + H_z \vec{e}_z$.

assumed to be incompressible, nonconducting, and to have a constant temperature and a homogeneous distribution of magnetic particles. Using the gap $d = r_2 - r_1$ as the length scale, the diffusion time $\tau_d = d^2/\nu$ as the time scale, scaling pressure with $\rho\nu^2/d^2$, the magnetic field $\vec{H}$, and the magnetization $\vec{M}$ with $(\rho/\mu_0)^{0.5}\nu/d$ (μ_0 is the magnetic constant, i.e., magnetic permeability of free space), the nondimensional governing equations are

$$\left(\partial_t \vec{u} \cdot\nabla\right) \vec{u} - \nabla^2 \vec{u} \nabla p = \left(\vec{M} \cdot\nabla\right) \vec{H} + \nabla \times \left(\vec{M} \times \vec{H}\right)/2, \nabla\cdot \vec{u} = 0 \tag{1}$$

The cylinders are considered to be of no-slip type with velocity boundary conditions

$$\vec{u}\ (r_1, \theta, z) = (0, \mathrm{Re}_1, 0) \text{ and } \vec{u}\ (r_2, \theta, z) = (0, \mathrm{Re}_2, 0), \tag{2}$$

where the inner and outer Reynolds numbers are $\mathrm{Re}_1 = \omega r_1 d/\nu$ and $\mathrm{Re}_2 = \omega r_2 d/\nu$, respectively.

2.1 Magnetization equations

In order to solve (1), one needs additional information about the magnetic particles themselves, in particular their properties and interaction with an applied magnetic field. Therefore, (1) is solved together with an equation that describes the magnetization of the ferrofluid. A first approximation is to use the equilibrium magnetization of an unperturbed state with a homogeneously magnetized ferrofluid at rest with the mean magnetic moments orientated in the direction of the magnetic field, $\vec{M}^{eq} = \chi\vec{H}$, where χ is the magnetic susceptibility of the ferrofluid, determined using Langevin's formula [21]. The ferrofluid considered for all simulations in this chapter is APG933 [22] with $\chi = 0.9$. However, a ferrofluid's magnetization is also influenced by the flow field. For the presented numerical simulations, an approach based on the model of Niklas [4–6] is used. Furthermore, a stationary magnetization near equilibrium considering a small perturbation at the equilibrium magnetization $\left(\left(\vec{M} - \vec{M}^{eq}\right)\right)$ and small relaxation times $\Omega\tau << 1$, where Ω is the absolute value of half of the vorticity Ω and τ is the magnetic relaxation time. In the near-equilibrium approximation, Niklas [4] determined the relationship between the magnetization $\vec{M}$, the magnetic field $\vec{H}$, and the velocity $\vec{u}$ to be

$$\vec{M} - M^{eq} = c_N \vec{\Omega} \times \vec{H} \tag{3}$$

with $\vec{\Omega} = \nabla\times \vec{u}\ /2$ being the vorticity and the *Niklas coefficient*

$$c_N^2 = \tau/\left(1/\chi + \tau\mu_0 H^2/(6\mu\Phi)\right) \tag{4}$$

where μ is the dynamic viscosity and Φ is the volume fraction of the magnetic material.

2.2 Ferrohydrodynamic equations of motions

The magnetization can be eliminated from (1) by using (3) in order to obtain the ferrohydrodynamic equation of motion [4]:

$$\left(\partial_t + \vec{u}\cdot\nabla\right)\vec{u} - \nabla^2\vec{u} + \nabla p_M = -c_N^2\left(\vec{H}\,\nabla\cdot\vec{F} + \vec{H}\times\nabla\times\vec{F}\right)/2 \tag{5}$$

where $\vec{F}=\vec{\Omega}\times\vec{H}$ and p_M are the dynamic pressure incorporating all magnetic terms which can be written as gradients. Note that the relaxation time τ could typically be defined by $\tau = \tau_B\langle D^3\rangle^{1/3}$, where τ_B is the Brownian relaxation time and $\langle D^3\rangle^{1/3}$ is the averaged diameter of the magnetic particles. For simplicity, to investigate the different effects, i.e., internal magnetization and elongational flow (see below), we assume that τ is constant, which is independent of the magnetic field $\vec{H}$. The considered relaxation time is based on the experimental result [22] ($\tau = \tau_{APG933}/\tau_d = 0.0018$).

Consider external field to be equal to internal one $\left(\vec{H}=\vec{H_{ext}}\right)$, (5) can be simplified to

$$\left(\partial_t + \vec{u}\cdot\nabla\right)\vec{u} - \nabla^2\vec{u} + \nabla p_M = -c_N^2\left(\vec{H}\,\nabla\cdot\vec{F} + \vec{H}\times\nabla\times\vec{F}\right)/2 \tag{6}$$

In this approach, the magnetic field and all the magnetic properties of the ferrofluid influence the velocity field only via the magnetic field, the *Niklas parameter* $\vec{s_N}=s_x\vec{e_x}+s_z\vec{e_z}$ [4–6], whereby magnetic field strengths are:

$$s_x = \left[2(2+\chi)/\left((2+\chi)^2-\chi^2\eta^2\right)\right]H_x c_N \text{ and } s_z = H_z c_n \tag{7}$$

In this approach, s_x and s_z are dimensionless numbers, describing the strength of the applied magnetic field.

3. Ferrofluidic flow under finite magnetic field

3.1 Introduction and motivation

We start our discussion with the investigation of the influence of a homogeneous magnetic field on a ferrofluid. In this first part, we will assume that the internal magnetic field is equal to the external applied magnetic field, i.e., homogeneous. Moreover, we ignore in this section any kind of finite size effects, e.g., possible agglomeration and chain formation, later considered as elongational flow effect (Section 4). Therefore, we consider the ferrofluid particles as point-size objects without any 3D expansion. Structure, dynamics, symmetry properties, bifurcation, and stability behavior of different vortex structures are investigated for axial and transversal magnetic fields, as well as combinations of them, i.e., oblique magnetic field. We will see that a transversal magnetic field has significant influence. It modulates and changes the classical flow structures, as well the basic state (Circular Couette flow, CCF) as the classical primary supercritical ones, Taylor vortex flow (TVF) and the spiral vortex flow (spirals, SPI). They are replaced by wavy-modulated flow structures: wavy Taylor vortex flow (wTVF) and wavy spiral vortex flow (wSPI), as well as they forward bifurcate out of the modified 2-fold circular Couette flow (2-CCF).

3.2 Flow structures

3.2.1 Flow structures in absence of a magnetic field

There are two fundamental basic, topologically different flow structures appearing in (classical) Taylor-Couette flow (see also Nomenclature and

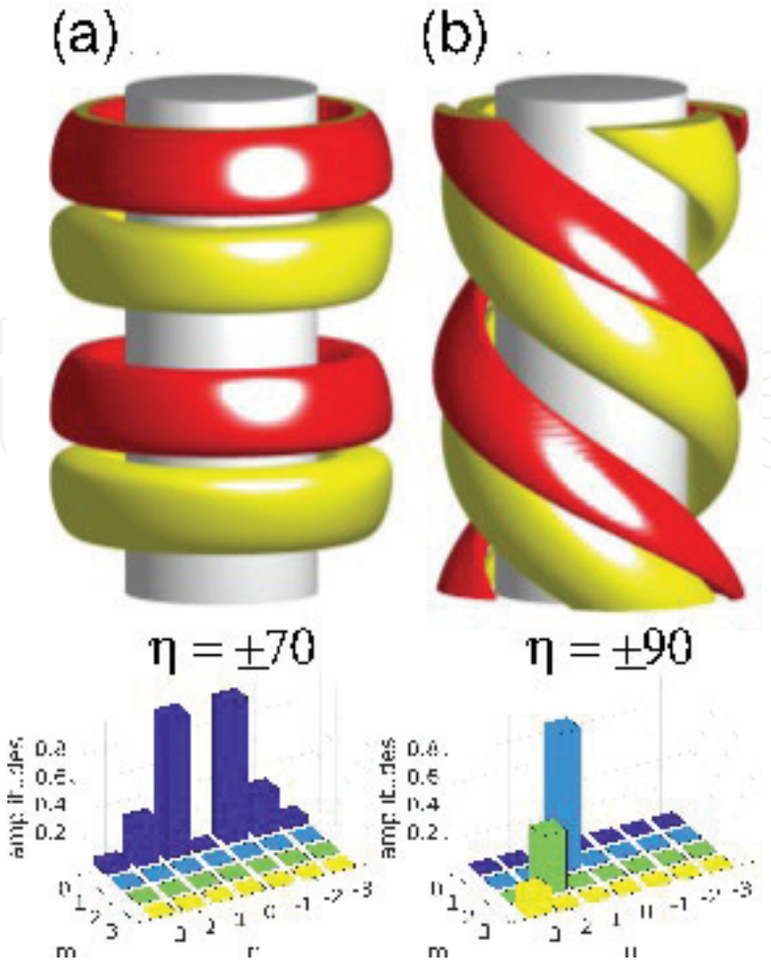

Figure 2.
Azimuthal vorticity isosurfaces η over two axial wavelengths (for visual purpose) in absence of a magnetic field (N) of (a) TVF at $\mathrm{Re}_2 = 0$, $\mathrm{Re}_1 = 100$, *and (b) SPI at* $\mathrm{Re}_2 = -150$, $\mathrm{Re}_1 = 150$. *Red (yellow) isosurfaces correspond to positive (negative) values as indicated. The bottom row shows mode amplitudes* $|u_{m,n}|$ *of the radial velocity field u corresponding to structures above over the m-n plane. The values are scaled regarding the maximum mode amplitude to be 1 (TVF:* $|u_{0,1}| = 1$*).*

abbreviations section). These are either toroidally closed Taylor vortices (Taylor vortex flow, TVF) and helical spiral vortices (spiral vortex flow/spirals, SPI) [20]. **Figure 2** shows the structure of these fundamental solutions, TVF and SPI (here for a left-handed SPI with azimuthal wavenumber $m = 1$), by using isosurfaces of the azimuthal vorticity. Because of the system symmetry $z \rightarrow -z$, we only discuss left-handed SPI. Without other parameters, e.g., axial through flow, left- and right-handed SPI are mirror images of each other. These pure states can also be found modulated as wavy structures, which are topologically identical with the pure states. However, they show a wavy-like deformation that results from additional and other stimulated modes compared to the classical solutions.

While *classical* wavy flow solutions [27–36] are well known and have already been widely discussed in literature regarding TCS, the ones generated by a magnetic field are different. In particular, the magnetically induced wTVF are *nonrotating* structures having a *pinned* phase, contrary to the classic wTVF, which *rotate* azimuthally. Regarding the flow structure, the imposed magnetic field shrinks and expands the vortices at different cross sections of constant θ, resulting in an azimuthal alternating wide and narrow vortex belly structure.

3.2.2 Flow structures—mode coupling in magnetic fields

Following, we will have a quick look at the impact on the different applied magnetic field with respect to the flow structures and in particular their mode

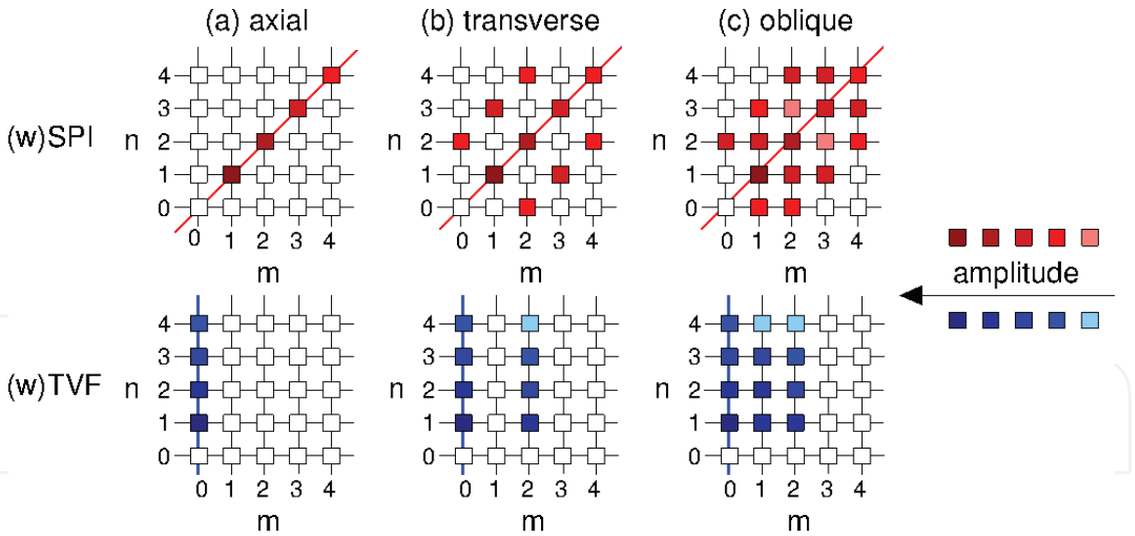

Figure 3.
Schematic sketch of modes in the presence of different externally imposed (homogeneous) magnetic fields. Here, m represents the azimuthal, and n the axial mode index in the Fourier expansion (Appendix (17) and (18)). (a) Modes either in absence of any magnetic field or in a pure axial magnetic field. (b) Pure transversal magnetic field with additional stimulation of $m = n \pm 2$ modes. (c) Superposition of axial and transversal fields with even further finite $m = n \pm 1$ modes. Strength of mode amplitudes, the magnitudes are characterized from dark (large amplitudes) to bright (small amplitudes) colors (legend right). Red and blue lines indicate the dominant mode amplitudes of the flow structures.

spectra. The modifications in NSE due to the additional terms incorporating magnetization and magnetic field result in various new phenomena. Most important is probably the fact that magnetic fields with a finite transversal component stimulate additional modes. Depending on different external applied magnetic fields, **Figure 3** presents a schematic plot for the different stimulated modes, depending on the applied field.

Having a *pure* axial field ($s_x = 0, s_z > 0$) applied the mode spectra, the flow structures remain qualitatively similar to the no field (N) case (**Figure 3(a)**). A TVF still contains only the axisymmetric modes $m = 0$ (with dominant n = 1, see also **Figures 2** and **6**). Similarly, L1-SPI, i.e., a left-handed SPI flow with azimuthal wavenumber $m = 1$ contains modes only on the diagonal $m = n$ (with dominant $n = 1$, see also **Figures 2** and **6**). However, if a field with finite transversal component is applied additional mode become finite and the flow structures change. A pure transversal field ($s_x > 0, s_z = 0$) excites $m = \pm 2$ modes lying on the secondary diagonal $m = n \pm 2$ (**Figure 3(b)**). Thus, as a result, the pure states of TVF and SPI vanish in the presence of a transversal magnetic field. They become wavy-like modified, resulting in wTVF and wSPI. Finally, having a magnetic field with either axial and transversal component ($s_x > 0, s_z > 0$), there are further interactions, which result in stimulation of additional $m = n \pm 1$ modes (**Figure 3(c)**). Moreover, these additional modes can induce further nonlinear mode couplings. As a result, the mode spectra contain more nonzero components (**Figure 3(c)** and **Figure 6** for numerical results). Thus all flow structures in a magnetic field with transversal component differ qualitatively from the classical flows found in the absence of magnetic fields [6, 26].

3.3 Effect of finite magnetic fields

3.3.1 Basic state and symmetries

If only a pure axial magnetic field, $H_{ext}(r)\vec{e_z}$ (see **Figure 1**), the classical circular Couette flow (CCF) is observed, with $\vec{u}_{CCF} = (0, Ar + B/r, 0)$, where

$A = (\mathrm{Re}_2 - \beta Re_1)/(1+\beta)$, and $B = \beta(\mathrm{Re}_1 - \beta Re_2)/(1+\beta)(1-\beta)^2$, is a solution of (5) as the associated vorticity $\vec{\Omega}_{ccf} = \nabla \times \vec{u}_{ccf}$ is parallel to the applied magnetic field and therefore all magnetic terms vanish. Although for magnetic fields that are orientated purely in the radial or azimuthal direction, the basic state changes but remains axisymmetric with deviations from CCF only having an azimuthal component [4, 23]. As a result, in all of these cases, the basic state is invariant to a number of symmetries (azimuthal rotation, mirror symmetry, and axial translation) whose actions on a general velocity field are

$$R_\Phi(u,v,w)(r,\theta,z,t) = (u,v,w)(r,\theta+\Phi,z,t),\ \Phi \in [0,2\pi], \tag{8}$$

$$K_z(u,v,w)(r,\theta,z,t) = (u,v,-w)(r,\theta,-z,t), \tag{9}$$

$$T_\alpha(u,v,w)(r,\theta,z,t) = (u,v,w)(r,\theta,z+\alpha\Gamma,t),\ \alpha \in N \tag{10}$$

On the contrary, for a field with a finite transverse component, the base state is no longer axisymmetric. Although the basic state remains invariant to T_α and a modified mirror symmetry K_z^H [24], a transverse magnetic field T breaks the continuous axisymmetry R_Φ, resulting in a basic state with discrete symmetry R_π, i.e., with azimuthal wavenumber $m = 2$ [24]. Following, we will refer to this modified 2-fold symmetric CCF as 2-CCF. It is important to mention that this $m = 2$ state is stationary [24], which is in contrast to the generic breaking of a $SO(2)$ symmetry which would result in a rotating wave.

3.3.2 Bifurcation behavior

As seen in Section 3.2, an applied magnetic field can stimulate additional modes and thus changes the Fourier mode spectrum of flow structures resulting in new solutions. The results are wavy-like modified flow states. It is to expect that these mode-stimulated modifications also influence and appear in the primary bifurcation thresholds of the solutions, as well as in their growth rate. Following, we will have a look at the bifurcation behavior of the different flow structures with the additionally field-induced modes explained in Section 3.3. In particular, we will focus on four different field configurations: *no field (N)* $(s_x = 0, s_z = 0)$; *pure axial field (A)* $(s_x = 0, s_z = 0.6)$; *pure transversal field (T)* $(s_x = 0.6, s_z = 0)$; and *oblique field (O)* $(s_x = 0.6, s_z = 0.6)$ ((7) for parameters s_x, s_z).

Considering these four, non, pure axial, pure transversal, and oblique magnetic fields, **Figure 4** illustrates the stable forward bifurcating branches of toroidally closed TVF and of wTVF solutions, respectively. **Figure 5** shows the bifurcation diagrams for helical SPI and wSPI in an analogous way. Note that the shown wavy-

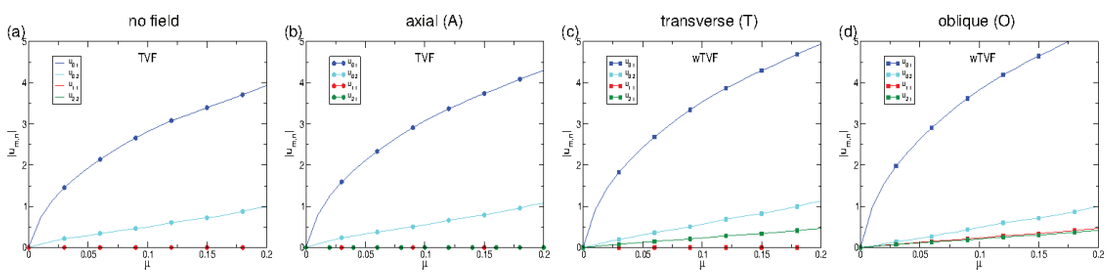

Figure 4.
Bifurcation diagrams of TVF and wTVF, respectively, in different magnetic fields: (a) no field (N), (b) axial (A), (c) transverse (T), and (d) oblique (O). Moduli $|u_{m,n}|$ (18) of the radial flow field amplitudes at mid gap are shown versus the relative distance $\mu = \mathrm{Re}_1/\mathrm{Re}_{1,c} - 1$ from the onset of the respective vortex flow. Further parameters are: $\mathrm{Re}_2 = 0, \beta = 0.5, k = 3.927$ *(cf.* ***Figure 2****).*

like modulated flow states only result from symmetry breaking due to finite transversal field component. In the **Figures 4** and **5**, the relative distance $\mu = \mathrm{Re}_1/\mathrm{Re}_{1,c} - 1$ is used as control parameter for easier comparison of the bifurcation branches ($\mathrm{Re}_{1,c}$ stands for the critical onset Reynolds number Re_1 of the flow structure, which depends on various system parameters. These are the aspect ratio Γ, the radius ratio r_1/r_2, the outer Reynolds number Re_2, axial boundary conditions, and the field strength s_x, s_z, respectively). The main reason to use μ is the shift in the bifurcation onset, which varies depending on the applied field direction.

Displayed in the **Figures 4** and **5** are the moduli $|u_{m,n}|$ of the dominant, as well as the first higher harmonic modes of the corresponding structure (see Appendix (18) and (19)), e.g. $(m,n) = (0,1)$ and $(m,n) = (0,2)$ for TVF. Furthermore, the largest field-induced mode amplitudes $|u_{2,1}|$ and $|u_{1,\pm 1}|$ (only in oblique configuration) of the wavy structures (cf. schematics in **Figure 3**) are included for comparison.

Axial field (A): As a pure axial magnetic field ($s_x = 0, s_z \neq 0$) does not stimulate any further modes within the mode-spectra (**Figure 3(a)**), the flow states TVF and SPI and their structural properties remain qualitatively similar, and they are as without a field. However, quantitative, they eventually change. First important effect is the rise of the onsets to higher values of Re_1 [6, 7]. Thereby, the upward shift depends on the various system control parameters (e.g., $\mathrm{Re}_2, \beta, \Gamma$). For parameters in **Figure 4**, the onset of TVF rises by about 25%, and for the parameters of **Figure 5**, the SPI bifurcation threshold moves upward in by about 15%. For the latter, consequently also corresponding SPI frequencies are increased in an axial field. Other change regarding **Figure 4** is the amplitude of the modes with increasing the parameter μ (weakest for nonfield and strongest for oblique field configuration).

Transversal field (T): A transversal magnetic field ($s_x \neq 0, s_z = 0$) stimulates additional azimuthal modes $m = n \pm 2$ (Section 3.2) as illustrated in **Figure 3(b)**. Thus, based on this knowledge, one can already expect a more dramatic influence on the classical TVF and SPI structures. As a pure axial field, a transversal field also delays the onset of the primary bifurcating structures, i.e., it stabilizes the basic state. Furthermore and more important is the fact that such a field also changes the flow structural properties in qualitative manner. The growth of the additional modulus $|u_{2,1}|$ (18) (for toroidally closed flow states) with $\mu = \mathrm{Re}_1/\mathrm{Re}_{1,onset} - 1$ changes the pure TVF to a wavy-like modulated wTVF. Analog pure SPI changes to wSPI (shown for L1-(w)SPI in **Figure 5**) due to the additional $m = n \pm 2$ (see **Figure 3(b)**), indicated by the growth of the modulus $|u_{3,1}|$ in **Figure 5**. It is worth to mention that due to the mode stimulation and interaction, also the (1,-1) mode becomes excited, which is similar to structure R1-(w)SPI. Note, the same also holds for the symmetry-related mirror image L1-(w)SPI.

Thus, in the presence of a magnetic field with a finite transversal component, the *pure/classical* TVF and SPI structures are modified. They are replaced by their

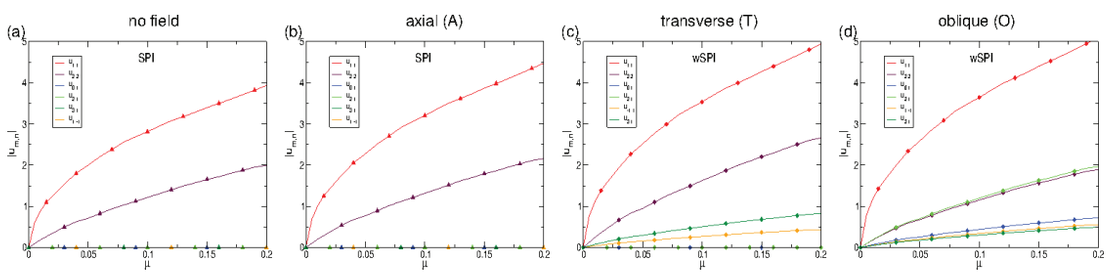

Figure 5.
Bifurcation diagrams of SPI and wSPI, respectively, in different magnetic fields: (a) no field (N), (b) axial (A), (c) transverse (T), and (d) oblique (O). Moduli $|u_{m,n}|$ (18) of the radial flow field amplitudes at mid gap are shown versus the relative distance $\mu = \mathrm{Re}_1/\mathrm{Re}_{1,onset} - 1$ from the onset of the respective vortex flow. Further parameters are: $\mathrm{Re}_2 = -150$, $\beta = 0.5$, $k = 3.927$ *(cf.* ***Figure 2****).*

wavy-like counterparts, wTVF and wSPI, which now bifurcate as *primary* structured solutions forward out of the CCF-2 ground state; note that already the basic state has an additional mode-2 symmetry due to the symmetry-breaking effect of the transversal field and as such already differ from the classical CCF (Section 3.3.1). As for axial field, the magnitude of stabilization varies with given system control parameters. In general, it is slightly smaller compared to the stabilization effect of an axial field. For instance for parameters presented in **Figures 4** and **5**, the upward shift for the onset of wTVF (wSPI) is about 20% (12%) in an axial (transversal) magnetic field.

Important to mention that a finite transverse component $s_x \neq 0$ breaks the system symmetry but does not change the degeneration between left- and right-handed SPIs. Both solutions keep bifurcating at the same critical values. The latter is different to the effect of an axial flow, for instance. Aside that such a flow also breaks the system symmetry, it separates both left- and right-handed SPI solutions. Under axial applied flow, they appear at different critical values.

Oblique field (O): As already seen for both pure field configurations, either $s_x \neq 0, s_z = 0$ or $s_x = 0, s_z \neq 0$, the onset of (w)TVF and (w)SPI is shifted to higher values. In fact in a field, obliquely orientated to the cylinder $(s_x \neq 0, s_z \neq 0)$, the magnitude of shift is bigger compared to the pure cases. In addition, as discussed before, such a superposition of an axial and a transversal field stimulates also new, additional modes with higher mode index combinations $m = n \pm 1$ (**Figure 3(c)** and for numerical simulations **Figures 4(c,d)**, **5(c,d)**, and **6(e,f)**).

A common finding for (w)TVF and (w)SPI is that their dominant mode amplitudes for $m = 0$ (for (w)TVF) and $m = 1$ (for (w)SPI) grow with respect to the bifurcation onsets. Although the absolute value depends on the different applied magnetic field, comparing the moduli $|u_{m,1}|$ at the same relative distance μ from the respective onset (**Figures 4** and **5**, compare dominant mode amplitudes), one finds the following relations

$$|u_{m,1}(s_x = c, s_z = c)| \geq |u_{m,1}(s_x = c, s_z = 0)| \geq |u_{m,1}(s_x = 0, s_z = c)| \geq |u_{m,1}(s_x = 0, s_z = 0)|$$

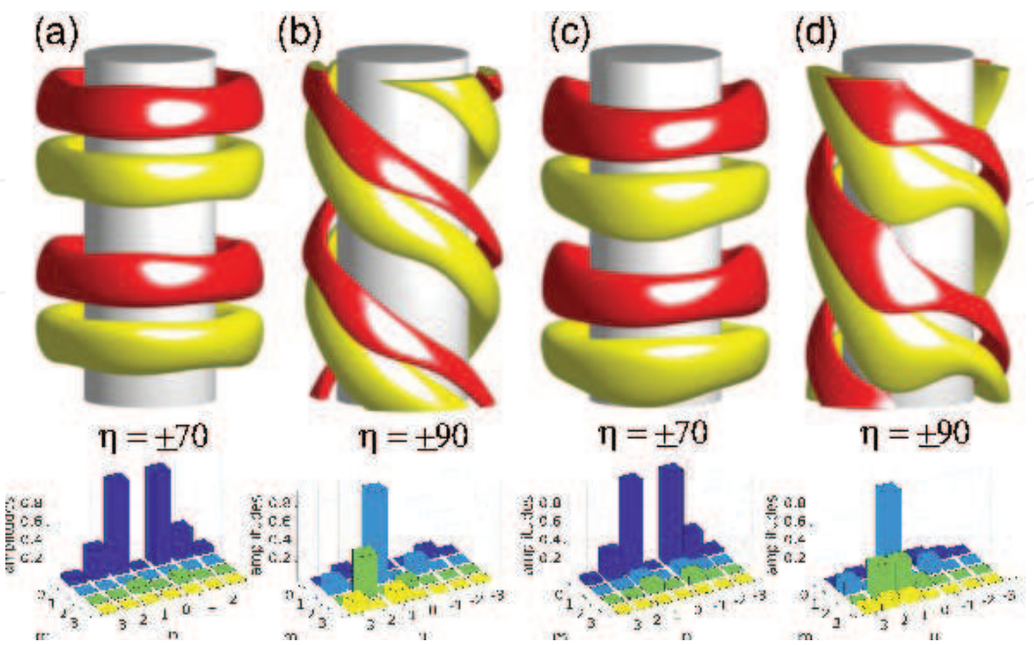

Figure 6.
Azimuthal vorticity isosurfaces η over two axial wavelengths (for visual purpose) with pure transversal applied magnetic field (T): (a) wTVF at $\mathrm{Re}_2 = 0$, $\mathrm{Re}_1 = 125$, *(b) wSPI at* $\mathrm{Re}_2 = -150$, $\mathrm{Re}_1 = 160$*; and oblique applied magnetic field (O): (c) wTVF at* $\mathrm{Re}_2 = 0$, $\mathrm{Re}_1 = 150$, *and (d) wSPI at* $\mathrm{Re}_2 = -150$, $\mathrm{Re}_1 = 190$. *Red (yellow) isosurfaces correspond to positive (negative) values as indicated. Bottom row shows mode amplitudes* $|u_{m,n}|$ *of the radial velocity field u corresponding to structures above over the m-n-plane. Values are scaled with the maximum mode amplitude to be 1 (TVF:* $|u_{0,1}| = 1$*).*

for a given constant value $c \in [0, 1]$ and $m = 0$ in case of toroidally closed (w)TVF and $m = 1$ for helical (w)SPI, respectively (Compare upper curves for dominant mode amplitudes $|u_{m,1}|$ in **Figures 4** and **5**).

For helical flow structures, the larger variety of mode interactions due to the basic spectra (e.g. $m = n$ [$m = -n$] for pure L1-SPI [R-SPI]) results in significant variation of the higher order and secondary stimulated modes, depending on the field configuration (see in particular **Figures 3(c)**, **4(d)**, and **5(d)**).

Based on the both bifurcation diagrams presented in **Figures 4** and **5**, it is worth to remind that in the case of a finite transversal field component $s_x \neq 0$, no pure solutions, TVF and SPI, exist. They become replaced by wavy-like modulated wTVF and wSPI. However, independent of the field, leading mode amplitude of the respective flow state, (w)TVF and (w)SPI, follows a typical square-root forward bifurcation, whereby the slope of its square grows with the applied field strength.

3.3.3 Vortex structures and mode contents

Having discussed the changes that different oriented magnetic fields can cause in the bifurcation behavior and mode stimulation of (w)TVF and (w)SPI, respectively, one can imagine that these also coincide with flow structural modifications. Now, we will address these structural changes of the vortices and the associated changes in the mode contents of the flows in more detail.

Figure 6 shows isosurfaces of the azimuthal vorticity η over two axial wavelengths (for visual purpose) for supercritical flow states (w)TVF and (w)SPI in the three different considered field configurations: (a,b) no field applied (N), (c,d) pure transverse field (T), and (e,f) oblique field (O) at parameters Re_1 and Re_2 as indicated.

A good quantity in order to visualize the field induced changes in the 3D vortex structures are isosurfaces of the azimuthal vorticity η. These surfaces appropriately convey structural details of the vortex flows in question [28].

Axial field (A): As a pure axial field does not break any continuous symmetry of the system, there is neither qualitative change in the structure of TVF and SPI in real space nor the mode structure of the flow in the $m - n$ Fourier plane (not shown, but similar as **Figure 2(a,b)**; only quantitative the mode amplitudes are slightly larger). TVF still consists of toroidally closed, rotationally symmetric vortex tubes with a mode spectrum containing only $m = 0$ modes (**Figure 2(a)**). And also, the helically oriented, open vortex tubes of SPI (here for left-winding spiral L-SPI) containing $m = n$ modes as shown in **Figures 2(b)** and **3** (mirror image of right-winding R-SPI analog) are *unaffected* by an axial field.

Transversal and oblique field (T, O): Having a magnetic field with finite transversal component crucially changes the scenario as TVF, and SPI structures are replaced by modified flow states due to the presence of such a magnetic field. In general, the isosurfaces become wavy-like deformed, and additional Fourier modes are stimulated as described before (Section 3.3; see also schematics in **Figure 3**). For pure transversal field, this mode stimulation results in wTVF with additional $m = \pm 2$ modes aside the $m = 0$ (**Figure 6(c)**) and in wSPI with $m = n \pm 2$ modes on the secondary diagonal(s) in addition to the $m = n$ SPI modes on the diagonal (**Figure 6(d)**). Beyond these, an oblique field further stimulates the modes $m = \pm 1$ in wTVF and $m = n \pm 1$ in wSPI due to more complex nonlinear dynamics/mode interaction. In particular, the spatio-temporal properties of the wTVF generated due to symmetry breaking magnetic field, either transversal or oblique (**Figure 6(c,e)**), differ significant from those of the classic wTVF. The structure of classical wTVF *rotates* as a whole in azimuthal direction [27, 32–35].

The wavy-like deformation on the toroidally closed vortices η introduced by a magnetic field with a finite transversal component is different. Regarding **Figure 6(c,e)**, one sees that the tubes of isosurfaces of the azimuthal vorticity become strong modified and bent at certain azimuthal cross sections of constant θ in comparison with the pure TVF tubes. Classic wTVF arises by deforming the TVF such that the axial stack of closed vortex tubes is wave-like modulated, bending axially upward and downward. Then, this deformation structure of the vortices rotates as a whole with a characteristic frequency. In contrast to these classical rotating wTVF, the wTVF initiated due to the symmetry-breaking transversal field component is *stationary* and does *not rotate* in azimuthal direction, instead, developing an 2-fold belly structure. It is worth to mention that such 2-fold symmetry also applies to the basic state. Thus, the classical rotational, axisymmetric CCF is replaced by the 2-CCF due to the symmetry breaking in the transversal magnetic field (see Section 3.2).

Consider wSPI, one can identify qualitative similar wavy characteristics, whereby the topological differences are weaker in comparison to wTVF. As the classical SPI structures already rotate without magnetic field, this also remains for wSPI in the presence of magnetic fields. However, also wSPI remains structural almost identical, and their modulation amplitude becomes enforced at certain cross sections of constant θ in presence of a transversal field component.

The basic state (CCF) loses stability either to (w)TVF (**Figure 5**) or (w)SPI (**Figure 6**). In case of wTVF, a supercritical pitchfork of revolution bifurcation breaks the axial translational symmetry T_α (8.3) and parameterizes the axial location of the steady axisymmetric family of solutions. On the other hand, (w)SPIs appear in a supercritical Hopf bifurcation which breaks the mirror symmetry K_z (8.2), resulting in a pair of symmetrically related spiral states, one with left-handed and the other with right-handed winding. It is worth to mention that a finite transverse magnetic field T breaks the axisymmetry R_φ, resulting in a basic state with discrete symmetry R_π, i.e., with azimuthal wave number $m = 2$ (section 3.3.1). Note that this $m = 2$ state is *stationary,* which is in contrast to a generic breaking of an $SO(2)$ symmetry, resulting in a rotating wave.

3.3.4 Stabilization of basic state: point of higher co-dimension

For TCS, a crucial point of special interest in the $\mathrm{Re}_1 - \mathrm{Re}_2$ phase diagram is the bicritical, co-dimension two point, γ, at which the primary bifurcation thresholds of TVF and SPI intersect/converge and as thus exchange the stability of the primary bifurcating solution [20]. For instance, in absence of a magnetic field and given wavenumber $k = 3.927$, the γ-point is given by $\mathrm{Re}_1 \approx 95.25$ and $\mathrm{Re}_2 \approx -73.69$ [28] (**Figures 7(a)** and **8(a)**); for smaller Re_2 (stronger counter-rotation), SPI bifurcate *stable,* and for larger Re_2 (less counter-rotation and co-rotation), TVF bifurcate stable respectively with increasing Re_1 (**Figure 8(a)**). Thus, with increasing Re_1, the 2nd solution bifurcates as *unstable* solution. Note that the γ-point is quite sensitive to the axial wavenumber; for different k, it moves toward higher Re_1 and smaller Re_2. This bifurcation scenario also holds for wTVF and wSPI in oblique and transversal magnetic fields.

It is worth to mention that the curves in **Figures 7(a)** and **8** present "*marginal stability*" thresholds. These are obtained for a fixed wavenumber $k = 3.927$, which differ from the '*critical*' thresholds. The latter is defined by the (smallest) Reynolds number, for which the flow structure first appears, which crucially depends on k. Thus, the intersection points of the curves for TVF and SPI (e.g., **Figure 7(a)**) are critical values, with respect to the fixed wavenumber.

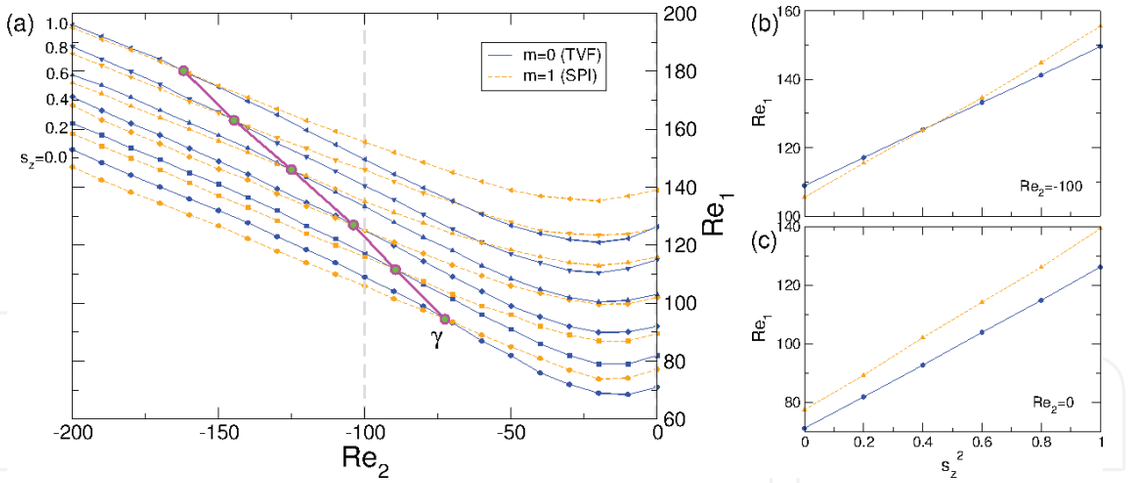

Figure 7.
(a) Influence of an axial magnetic field on the location of the bifurcation thresholds of TVF and SPI out of CCF in the $\mathrm{Re}_1 - \mathrm{Re}_2$ *diagram. Blue (full) lines refer to TVF and orange (dashed) ones to SPI. Magenta line with points indicates the moving of the* γ*-point with* s_z *towards smaller* Re_2*. Further shown are the bifurcation thresholds* $\mathrm{Re}_{1,c}$ *with increasing* s_z^2 *for fixed (b)* $\mathrm{Re}_2 = -100$ *and (c)* $\mathrm{Re}_2 = 0$*, respectively, obtained by full non-linear simulations.*

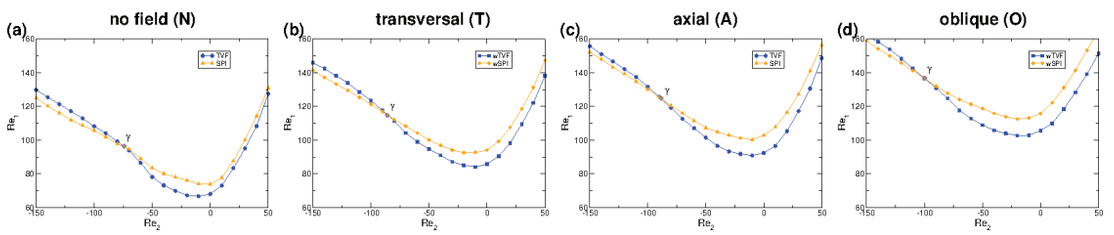

Figure 8.
Bifurcation curves for the onset of (w)TVF (blue) and (w)SPI (orange) in $\mathrm{Re}_2 - \mathrm{Re}_1$ *diagram under (a) no magnetic field (N)* $(s_x = 0, s_z = 0)$*, (b) an applied transverse field (T)* $(s_x \neq 0, s_z = 0)$*, (c) an applied axial field (a)* $(s_x = 0, s_z \neq 0)$*, and (d) an applied oblique field (O)* $(s_x \neq 0, s_z \neq 0)$*. Simulation results of full nonlinear Eqs. (11) consider short periodic TCS with* $k = 3.927$ *(cf. [6, 28]).*

Figure 7(a) illustrates an example for the influence of different axial magnetic field strength s_z on the bifurcation thresholds for TVF and SPI and the variation on the location of this bicritical γ point. These are results of linear calculations and were obtained with a shooting method [7]. Solid blue (dashed orange) lines refer to TVF (SPI). Note that always the lower (in $\mathrm{Re}_{1,c}$) bifurcating vortex solution is stable and the upper one is unstable. As discussed in Section 3.2, increasing s_z stabilizes the CCF basic state, both, against TVF and SPI, i.e., the upward shift of the respective threshold curves. In general, the strength of the stabilization effect is larger for helical SPI vortex structures than for toroidally closed TVF (e.g. **Figure 8**). As a result, the γ-point moves toward more negative Re_2 (i.e., toward the left in **Figure 7(a)**). Thus, it is observed that the Re_2 region of primary, stable bifurcating TVF expands with increasing s_z.

The same scenario also applies for transversal and oblique magnetic field configuration, whereby the magnitude of the shift is biggest for a pure axial magnetic field and almost equal for a pure transversal and oblique magnetic field (slightly larger for the latter). **Figure 7(b,c)** displays the bifurcation thresholds $\mathrm{Re}_{1,c}$ for fixed outer cylinder rotations, $\mathrm{Re}_2 = -100$ and $\mathrm{Re}_2 = 0$ with increasing s_z^2, resulting from fully nonlinear simulations. The slopes in **Figure 7(b,c)** depend crucially on Re_2. However, in general, the slopes for SPI are steeper than for TVF. For small to moderate field parameters, TVF is the primary stable bifurcating structure while

SPI bifurcate secondarily and unstable. For stronger fields, the structures interchange stability and bifurcation order.

Summarizing, for fixed Re_2, an axial field shifts the onset of helical SPI more strongly than the one of toroidally closed TVF. We furthermore found this behavior to appear for all parameters and magnetic fields: either for axial, transversal, and oblique magnetic fields (**Figure 8**). In this case, that for transversal and oblique fields, all structures are wavy-like modulated; wTVF and wSPI, respectively (see also Section 3.2).

In pure axial or pure magnetic fields, the upward shifts of the bifurcation values, the stabilization of the basic state (CCF or 2-CCF), i.e., the onset of the primary stable flow state (w)TVF or (w)SPI grows linearly (**Figure 7(b,c)**) with the squared magnetic field parameters s_x^2 or s_z^2, respectively [6]. Thereby, the magnitude of stabilization shift depends crucially on Re_2, in general is largest close to outer cylinder at rest.

3.3.5 Marginal stability thresholds: Stabilization of the basic state

Before going into detail about the stabilization of the basic state it is worth, once more to mention, that the basic state can be different in presence of a magnetic field, whether the field contains a symmetry breaking transversal component or not. For pure axial field, one finds the classical CCF which becomes replaced by the 2-fold symmetric 2-CCF for fields with finite transversal component (see also Section 3.3.1).

Figure 8 presents bifurcation thresholds for vortex flows under the influence of different magnetic fields. Shown is the $\mathrm{Re}_2 - \mathrm{Re}_1$ diagram, along which the CCF state loses stability. For comparison, (a) shows the thresholds in absence of any field $(s_x = 0, s_z = 0)$, while the same thresholds are shown for (b) a transversal $(s_x \neq 0, s_z = 0)$, (c) an axial $(s_x = 0, s_z \neq 0)$, and (d) an oblique field $(s_x \neq 0, s_z \neq 0)$. These results were obtained by nonlinear simulations with the full field ferrohydrodynamical Eqs. (11), considering a short periodic TCS with $k = 3.927$. See also **Figure 7**, for linear stability analysis, in which the shift of the higher co-dimension γ-point is shown together with stabilization of CCF in an axial field.

For all bifurcation thresholds of TVF, SPI, wTVF, and wSPI upward shifts of the bifurcation values, $\mathrm{Re}_{1,c}$, as shown in **Figure 8**, are observed. However, the exact onsets of the different primary bifurcating structures differ, either depending on the particular applied field as well as on Re_2.

In absence of a magnetic field (**Figure 8(a)**) and sufficiently strong counter rotation, $\mathrm{Re}_2 \leq -73$ [28], the basic state, CCF, first becomes unstable to a helical solution, SPI, in a supercritical Hopf bifurcation breaking K_z, which results in a pair of symmetrically related, degenerated spiral states, one with left-handed winding and the other with right-handed winding. For considered Re_2-parameter range in **Figure 8**, the bifurcating SPI has an azimuthal wavenumber $m = 1$ (or $m = -1$ in case of the right-handed SPI). Note that the wavenumber m of the primary bifurcating SPI increases with stronger counter-rotating cylinders [20]. On the other hand, for $\mathrm{Re}_2 \geq -73$, the basic state loses stability to the toroidally closed TVF. The supercritical pitchfork of revolution bifurcation breaks T_a, and the steady axisymmetric family of solutions are parametrized by their axial location.

Considering a pure axial magnetic field, the scenario remains mainly unchanged (**Figure 8(c)**); still SPI and TVF appear as primary supercritical flow states with an intersection of the bifurcation thresholds at a specific value Re_2. As already seen in **Figure 7**, increasing field strength s_z in a pure axial field tends to shift the

co-dimension γ-point toward more negative Re_2. The same also holds for increasing s_x in a pure transversal field, with significant minor effect on Re_2 variation. Thus, the magnetic fields tend to render the corresponding basic states more unstable to (w)TVF and more stable to (w)SPI, respectively.

Having a field with finite transversal component, either pure transversal (**Figure 8(b)**) or oblique orientated (**Figure 8(d)**), the primary instabilities, with TVF being replaced by wTVF, and SPI being replaced by wSPI, respectively, just as the basic states were modified from CCF to 2-CCF due to the presence of the magnetic field. Their onset $\mathrm{Re}_{1,c}$ occurs at higher Re_1 values for any given Re_2 value compared to the onset of classical TVF and SPI in the absence of a magnetic field. Thus, the magnetic fields alter the basic states and make them more robust to instabilities. The level of stabilization is greater for a pure axial field compared to a pure transversal field, but strongest, when an oblique field is imposed (bifurcation values $\mathrm{Re}_{1,c}$ grow with field parameters s_x, s_z).

An oblique magnetic field results in the strongest upward shift of bifurcation values $\mathrm{Re}_{1,c}$, and also, this shift depends on Re_2, which interestingly is largest about $\mathrm{Re}_2 = 0$, outer cylinder at rest. Furthermore, the topological different flow structures of (w)TVF and (w)SPI are shifted about the same amplitude, with a slightly lager effect on helical (w)SPI for the considered $\mathrm{Re}_2 - \mathrm{Re}_1$ diagram. This should be kept in mind regarding later consideration involving field modulation via internal dependence, presented in Section 5.

So, while a pure axial fields shift the bifurcation onsets more strongly (i.e. to larger values Re_1) than pure transversal ones (**Figure 8**), the latter one has a stronger influence on the nonlinear spatio-temporal properties and dynamics of the bifurcating vortex structures (**Figure 6**). Combining both portions to an oblique field enforces both effects. One finds either larger shifts as well as stronger modulated flow structures (**Figure 6(e,f)**).

3.4 Resume

An external applied magnetic field (independent of its orientation) *stabilizes* the CCF (2-CCF) basic state: for a given value of the outer Reynolds number Re_2, the bifurcation thresholds $\mathrm{Re}_{1,c}$ for vortex structures are shifted to higher values of the inner Reynolds number Re_1. This holds likewise for toroidally closed (w)TVF, as well for helical (w)SPI. Thereby, these shifts are typically linear in the squared field parameters s_x^2 or s_z^2, respectively. Moreover, stabilization is in general stronger for helical solutions (w)SPI than for toroidally closed ones (w)TVF. Additionally, an external applied magnetic field can, depending on its orientation, change the spatio-temporal structure of the classical TVF and of SPI. The reason is the stimulation of additional modes entering the axial and azimuthal Fourier decomposition of the flow. A pure axial magnetic field keeps the symmetry properties unchanged and does not change the flow structures. It only alter the flow amplitudes, i.e., the magnitude of up-shift in the onsets and magnitude of modes after bifurcation. On the other hand, as soon as a *finite transversal* field component is present (pure transversal or oblique field), all flow structures become always *3-dimensional* and therefore qualitatively different to the classical TVF and SPI states. In particular, they are wavy-like modulated and the pure structures do *not* exist anymore. Such a field component breaks the system symmetry and therefore alters either basic state (CCF changes to 2-CCF) and supercritical instabilities. As a result, one finds new solutions, field generated, *nonrotating* wTVF, contrary to the classical rotating ones. The vortex tubes of these wTVF are periodically expanded and constricted in azimuthal θ-direction, and this deformation pattern is *stationary*. In general, the

bifurcation thresholds $\mathrm{Re}_{1,c}$ for non-axisymmetric, helical $m = 1$ (w)SPI are stronger modified in presence of a magnetic field than those for toroidally closed $m = 0$ (w)TVF. The upward shift towards larger values of Re_1 of the former is bigger than for the latter. One direct effect is the shift of the co-dimension point toward stronger counter-rotating frequencies. This effect has been found to show in axial, transversal, and oblique magnetic fields [6, 9].

Finally it is worth to mention that the magnetic field (transversal or oblique field) generated wTVF differ crucially from the classic wTVF [20, 33, 35, 45] that bifurcates *secondary* out of TVF at relatively high $\mathrm{Re}_{1,c}$ in absence of a magnetic field. The present generated wTVF arises via a *primary* bifurcation directly out of the 2-CCF basic state.

4. Agglomeration and elongational flow effects

4.1 Introduction and motivation

Aside the general difficulties to incorporate the magnetization of any magnetic field into the governing equations of motion, it is also crucial to consider the specific properties of the magnetic particles. However, most mathematical models describing the flow of complex magnetic fluids typically assume noninteracting magnetic particles with a *small* volume or only *point-size* objects. However, real ferrofluids consist of a suspension of particles with a *finite size* in an almost ellipsoid shape. Moreover, they involve *particle-particle interactions* resulting in agglomeration; in particular, they tend to form chains of various lengths. One possibility to include such effects and to come close to the realistic situation for ferrofluids is to consider the effect of *elongational flow*. Mathematically, such flow is incorporated by the symmetric part of the velocity gradient field tensor, which could be scaled by a so-called, material dependent, *transport coefficient* λ_2 [10, 37, 38]. As discussed in the previous section, magnetic fields tend to change the bifurcation threshold of the supercritical unstable flows and, depending on their orientation, resulting in structural modifications. Consider elongational flow, these modifications are expected to change the obtained states at least qualitatively.

4.2 Modified internal magnetic field

In order to consider such *elongational flow* (i.e. agglomeration, chain formation, etc.), one has to determine the relationship between the magnetization $\vec{M}$, the magnetic field $\vec{H}$, and the velocity $\vec{u}$. One possibility is to consider an additional dependence of the magnetization on the symmetric part of the velocity gradient $S = \left(\partial_i u_j + \partial_j u_i\right)/2$ [10, 38]. Thus, the magnetization (4) becomes modified to

$$\vec{M} - \vec{M}_{eq} = c_N \vec{G} \tag{11}$$

where $G = \vec{\Omega} \times \vec{H} + \lambda_2 S \vec{H}$.

Onsager symmetry relations then require [12, 39] that additional forces involving λ_2 appear in the off-equilibrium momentum balance of the ferrofluid.

Now, using the latest modified magnetization (9), the magnetization part in (1) can be eliminated, similar to previous discussion in Section 2.2. We thus have the following ferrohydrodynamic equation of motion (including elongational flow effects) [12]:

$$\left(\partial_t + \vec{u}\cdot\nabla\right)\vec{u} + \nabla p_M - \nabla^2\vec{u} = -c_N^2\left[\vec{H}\,\nabla\cdot\vec{G} + \vec{H}\times\nabla\times\vec{F}\right]/2 \tag{12}$$

where p_M is the dynamic pressure incorporating all magnetic terms which can be written as gradients, i.e., $\nabla\left(\vec{H}\cdot\vec{H}\right)$ and $\nabla\left[\left(\vec{H_{eq}} - \vec{H}\right)\cdot\vec{M}\right]$. See also (5) for comparison *without* considered elongational flow.

Assuming that the internal magnetic field is equal to the external imposed magnetic field (it is known as a leading-order approximation [24], see also following section 5) which is sufficiently good for a 'first' numerical investigation for the effect of elongational flow. Therefore, (10) can be simplified:

$$\begin{aligned}\left(\partial_t + \vec{u}\cdot\nabla\right)\vec{u} + p_M - \nabla^2\vec{u} = s_N^2\Big\{&\nabla^2\vec{u} - 2\lambda_2\nabla\cdot S\vec{H} - H\\ &\times\left[2\nabla\times\left(\vec{\Omega}\times\vec{H}\right) - \vec{H}\times\nabla^2\vec{u} + \lambda_2\nabla\times S\vec{H}\right]\Big\}\end{aligned} \tag{13}$$

In this approach, the magnetic field and all the magnetic properties of the ferrofluid could be influenced by the velocity field, the transport coefficient λ_2, and the magnetic field Niklas parameters s_x and s_z as described before (7). However, it is worth to mention that in this approach, the material dependent transport coefficient λ_2 is a parameter [12], which can be scaled by the term describing the elongational flow and is *independent* of $\vec{H}$. Thus, it only appears in combination with the symmetric component of the velocity field tensor. However, real ferrofluids show $\vec{H}$ dependence in the microscopic aspect of the dynamics of ferrofluids with chains or nonspherical particles [25].

4.3 Linear stability behavior and analysis

Before we come to the influence of λ_2 onto the fully nonlinear Eqs. (11), it is worth to have a look at the linear marginal stability threshold of the different flow structures. Therefore, in the following, we first investigate the linear growth behavior of either stationary axisymmetric $m = 0$ (TVF) and nonaxisymmetric $m = 1$ (SPI) oscillatory vortex flow of a ferrofluid in the TCS that is placed in homogeneous axial magnetic fields $\vec{H}_{ext} = H_z\vec{e}_z$ (**Figure 1**). In the literature [4, 5, 7, 40–42], one can find many theoretical works that analyze (via linear stability analysis) the influence of rotational symmetric magnetic fields, i.e., axial, azimuthal, and radial ones on the flow of a ferrofluid in the TCS. However, for a symmetry breaking (e.g., transverse), magnetic field such linear stability analysis is *not known* for the corresponding basic state at such a field configuration. For a detailed description regarding the linearization around the CCF and solution of the linearized NSE, we refer to the Appendix in [43].

4.3.1 Marginal stability thresholds

In order to discuss how the transport coefficient λ_2 influences the growth of $m = 0$ and $m = 1$ vortex perturbations, we determine the stability of the CCF basic state against these perturbations, considering a magnetic field $\vec{H}_{ext} = H_z\vec{e}_z$, applied in pure axial direction.

Figure 9 presents the bifurcation thresholds in the $\mathrm{Re}_2 - \mathrm{Re}_1$ diagram for either axisymmetric, $m = 0$, and nonaxisymmetric, $m = 1$, vortex flow in magnetic fields at (a,b) $H_{ext} = 67.7\,kA/m$ and (c) $H_{ext} = 135.4\,kA/m$ for two different axial

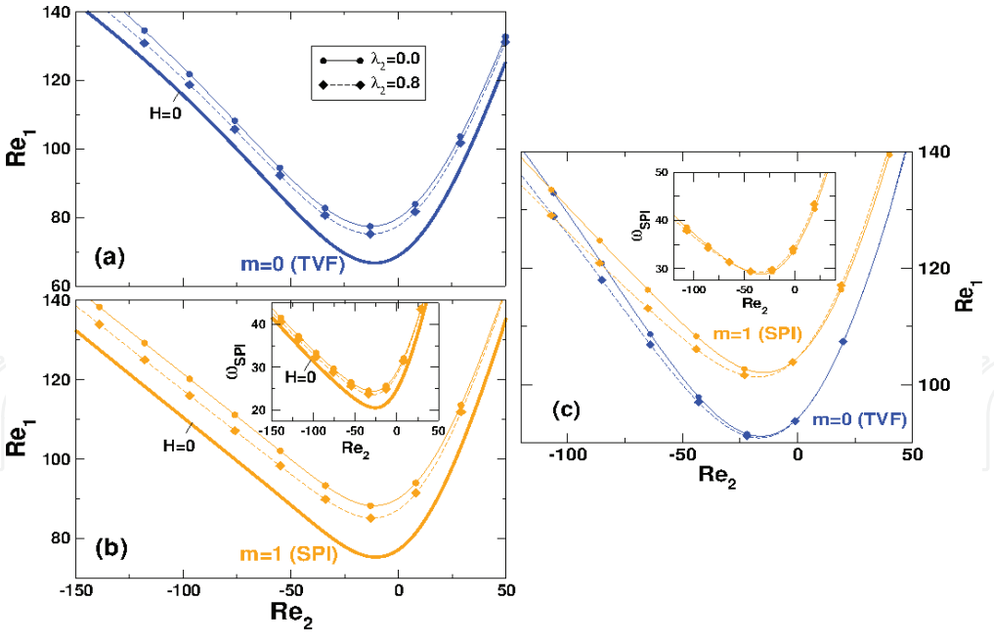

Figure 9.
Stability thresholds of the CCF basic state against vortex growth of (a) $m = 0$ (TVF) and (b) $m = 1$ (SPI) in the $\mathrm{Re}_2 - \mathrm{Re}_1$ diagram of control parameters. Thin solid and dashed lines with symbols show the results for $\lambda_2 = 0$ and $\lambda_2 = 0.8$ for a magnetic field $H_{ext} = 67.7kA/m$. The axial wavenumber is $k = 2.8274$. (c) Same curves, with wavenumber $k = 3.4558$ and magnetic field is $H_{ext} = 135.4kA/m$. The lowest thick curve in (a) and (b) refers in each figure to the threshold in absence of a magnetic field $H_{ext} = 0$. Insets show corresponding SPI frequencies at the bifurcation thresholds.

wavenumbers. Note that the representative axial wavenumber chosen in (a) $k = 2.8274$ is as detected in experiments [10]; (b) $k = 3.4558$. Insets in **Figure 9(b,c)** show corresponding SPI frequencies at the bifurcation thresholds. As already discussed in Section 3.3.4, the CCF basic state is stabilized against the two types of vortex perturbations in any magnetic field (the lowest thick solid curve in each plot in **Figure 9** refers to the case without any magnetic field H = 0 (c.f. **Figure 8(a)** for nonlinear calculation)). Consider elongational flow ($\lambda_2 \neq 0$), the basic state becomes destabilized in comparison with the case $\lambda_2 = 0$. Regarding **Figure 9(a,b)**, both bifurcation thresholds for $m = 0$ and $m = 1$ vortices are shifted to *lower* values of Re_1. Thus, for the axial wavenumber of $k = 2.8274$, the λ_2 term *reduces* the general stabilization effect caused by an applied magnetic field. For parameters as presented in **Figure 9(a,b)**, this holds for the whole range of presented Re_2, even when the changes of the stability boundaries are quite weak, in particular for corotating cylinders. It is important to mention that it never over-compensate the field induced stabilization. **Figure 9(c)** illustrates in general a strong parameter dependence of the elongational flow effect. While at $\mathrm{Re}_2 < 22$ for TVF and $\mathrm{Re}_2 < 4$ for SPI, increasing λ_2 also has destabilizing effect, and for corresponding larger Re_2, the effect is just *opposite*. Increasing λ_2 even enforce the stabilization due to the applied magnetic field.

It is worth to mention that, in contrast to the stabilization of the CCF state by a magnetic field, the λ_2-induced modifications of the linear growth of vortices depend significantly on their axial wavenumber k as will be discussed below.

4.3.2 Magnetic field dependence of thresholds

Figure 10(I) illustrates the variation of the bifurcation thresholds $m = 0$ (TVF) and for $m = 1$ (SPI) with the magnetic field $\vec{H}_{ext} = H_z \vec{e}_z$, incorporating the elongational flow effect. The top row of figures refers to $\mathrm{Re}_2 = 0$, and the bottom one to $\mathrm{Re}_2 = -100$ and wavenumbers are $k = 2.8274$ (left) and $k = 3.1415$ (right),

respectively. Ignoring the effect at small H_{ext}, all thresholds increase linearly with H_{ext}. The slopes are given by $\partial \mathrm{Re}_{1,stab}(H)/\partial H$ and vary slightly either with λ_2 and k. For outer cylinder at rest, $\mathrm{Re}_2 = 0$, (**Figure 10(I)(a)**) the slopes of the $m = 0$ and $m = 1$ curves are comparable, they differ significantly for counter-rotating cylinders, $\mathrm{Re}_2 = -100$ (**Figure 10(I)(b)**). For the latter, this results in intersections of the $m = 0$ and $m = 1$ stability boundaries. Such intersections have been observed also in experiments and also in full nonlinear simulations [6] with $\lambda_2 = 0$.

In general, modifications of the H_{ext} field dependence of the bifurcation thresholds due to λ_2 tend to increase, when the cylinders are stronger counter-rotating (**Figure 10(I)**). Re_2 becomes more negative, and thus, the strain increases. On the other side, they also depend on the axial wavenumber k (see also Section 4.3.4). Considering fixed k, the modifications due to λ_2 increase with increasing magnetic field H_{ext} while remaining qualitatively the same. However, the general tendency visible in **Figure 11**, considering elongational effect, is to shift the stability boundaries downward in Re_1. Concrete amounts depend on the parameters k and Re_2. Note that this relative small destabilizing elongational effect is always overcompensated by the significant stronger general stabilization effect of the magnetic field itself.

4.3.3 Frequencies of helical SPI states

Instead of looking at the growth rates—the real part of the eigenvalue of these solutions (previous Sections), one can also consider the marginal spiral frequency ω—the imaginary part of the marginal eigenvalue at the bifurcation threshold of $m = 1$ (SPI) vortex flow. **Figure 10(II)** shows the frequency, corresponding to the $m = 1$ bifurcation thresholds presented in **Figure 10(I)**. Main effect is the increase of the SPI frequencies with the field H_{ext}, accordingly to the increase of onset Reynolds numbers with H_{ext} (**Figure 10(I)**). Thus, the threshold frequencies are larger for $\mathrm{Re}_2 = -100$ than for $\mathrm{Re}_2 = 0$. In general, the effect induced by elongational flow is minor, significant smaller, and only secondary. Analog to the slightly down shift in the onsets (**Figure 10(I)**) also the SPI frequencies are slightly reduced (**Figure 10(II)**). Strong counter-rotating cylinders reduce in general the frequency for finite λ_2 (**Figure 10(II)**), while for larger wavenumbers, a finite elongational flow $\lambda_2 \neq 0$ at $\mathrm{Re}_2 = 0$ it can be slightly decreased.

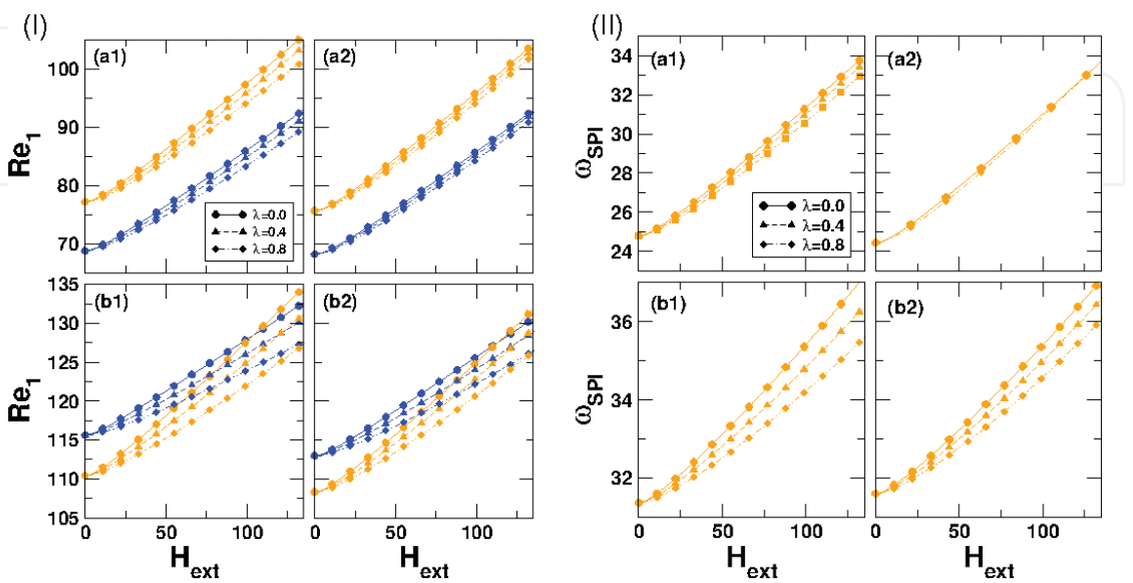

Figure 10.
(I) Variation of the (a) $m = 0$ (TVF) and (b) $m = 1$ (SPI) bifurcation thresholds and (II) corresponding SPI frequencies ω with magnetic field H_{ext} for different λ_2 as indicated. The top row refers to $\mathrm{Re}_2 = 0$ and the bottom one to $\mathrm{Re}_2 = -100$. The wavenumbers are (1) $k = 2.8274$ and (2) $k = 3.1415$, respectively.

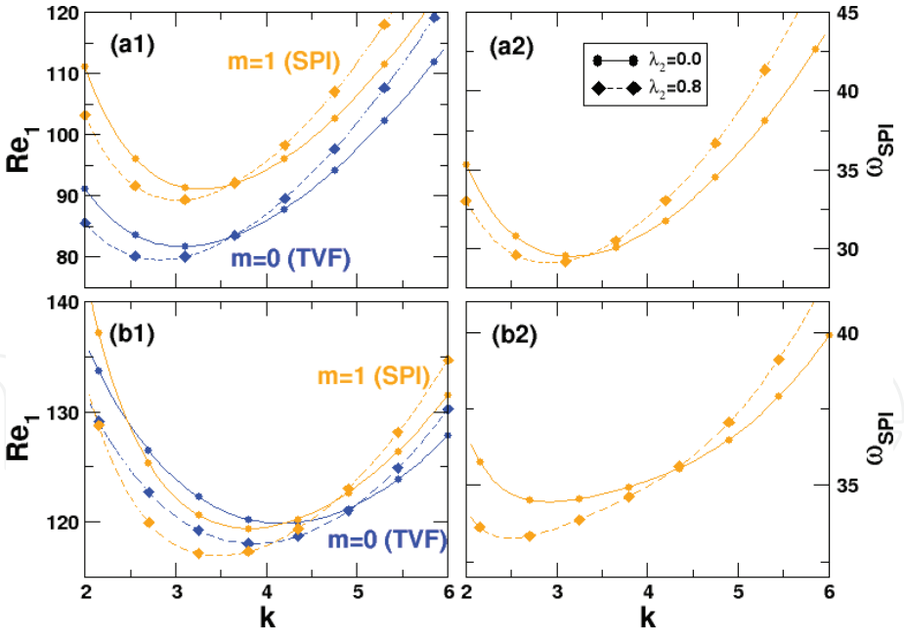

Figure 11.
(1) Stability boundaries of the CCF basic state against the growth of $m = 0$ (TVF) (blue) and $m = 1$ (SPI) vortex flow (orange) in the $k - \mathrm{Re}_1$ diagram for $\lambda_2 = 0$ (solid lines) and $\lambda_2 = 0.8$ dashed lines. (2) corresponding marginal spiral frequencies ω at the $m = 1$ thresholds. Further parameters: (a) $\mathrm{Re}_2 = 0$ and (b) $\mathrm{Re}_2 = -100$. The (axial) magnetic field is constant with $H_{ext} = 80kA/m$. Results from linearized equations [43].

A general observation is that all modifications of the spiral frequencies due to finite $\lambda_2 \neq 0$ are most pronounced for the smaller wavenumbers (here $k = 2.8274$ in **Figure 10**) in counter-rotating cylinders. The field dependence is virtually not much modified due to variations in λ_2, and the growth rate of the imaginary part of the marginal eigenvalue with increasing λ_2 is quite similar to that of its real part.

4.3.4 Axial wavenumber dependence

Following, we will first discuss the situation for a (moderately) larger wavenumber, taking $k = 3.4558$ as one specific, representative example. For larger value k (**Figure 9(c)**), the situation becomes more complicate. Incorporating the elongational flow scaled by the parameter λ_2 increases and decreases the growth rate, with respect to $\lambda_2 = 0$, and thus shifts the stability boundaries, up or down, depending on Re_2.

Figure 11 illustrates the relation between the wavenumber dependence of the stability boundaries and of the spiral frequencies. This is of particular interest in experiments, since the wavenumbers of some vortex structures show a strong variation when changing the magnetic field [9, 44]. Reindl *et al.* [9] also observed hysteresis between vortex flows with different k when increasing and decreasing the Reynolds numbers Re_1. The bifurcation thresholds (**Figure 11**, top row $\mathrm{Re}_2 = 0$ and the bottom row $\mathrm{Re}_2 = -100$; the (axial) magnetic field is fixed at $H_{ext} = 80\ kA/m$) for $m = 0$ and $m = 1$ vortex flow structures in the $k - \mathrm{Re}_1$ diagram change when the elongational term $(\lambda_2 \neq 0)$ is considered in the linearized ferrofluid equations [43]. Right column of **Figure 11(2)** presents the wavenumber dependence of the corresponding marginal spiral frequencies at the onsets for $m = 1$ SPI.

Typically, the thresholds for $\lambda_2 \neq 0$ (in **Figure 11** the case of $\lambda_2 = 0$, lines with squares) are shifted downward in Re_1 at smaller wavenumbers k and upward at larger k. Resulting in a fixed magnetic field, the elongational effect destabilizes (stabilizes) the CCF state against growth of vortices with small (large) wavenumbers, either for $m = 0$ or $m = 1$ perturbations. Consequently, the stability onsets cross for different values of λ_2 ($\lambda_2 = 0$, $\lambda_2 = 0.8$ in **Figure 11**) at a specific value of k_{cross} the wavenumber.

It is worth to mention that the crossover values of k_{cross} for $m = 0$ and $m = 1$ perturbations also depend sensitive on other the control parameters, e.g., Re_2. Based on the observations in **Figure 11**, it is fair to assume that, depending on the wavenumber k, the γ-point (Section 3.3.4) will change.

Similar to the stability thresholds, also the spiral frequencies (**Figure 11(2)**) increase with increasing λ_2 when k is large and decrease for smaller k as a result of switching on the elongational effect. Thereby, the crossing wavenumber, k_{cross}, separating the increase and decrease in ω is slightly smaller than the one for crossing the marginal thresholds (**Figure 11(a1,b1)**). Following the speculation by Odenbach and Müller [10] on the physical origin of the elongational effect, one can give a reasonable explanation for such an observed wavenumber dependence of the λ_2 effect on the growth rates of vortex flow. In [10], the authors argue that the microscopic origin of a finite λ_2 might be attributed to the finite asphericity of the colloids, i.e., the presence of (short) particle chains in the ferrofluid. Small axial wavenumber k will allow these chains *more easily* to remain aligned in the direction of the magnetic field in vortex flows instead in a flow with large axial wavenumber and large azimuthal vorticity. Larger wavenumber means smaller wavelength and therefore more higher probability to *unalign* in the given field. Thus, since the magneto-rotational dissipation in the latter flow is larger than in the former one, it requires larger centrifugal forces, i.e., larger values of Re_1, to drive the growth of a large k flow. However, it is important to state that this argumentation also holds some weakness: In the presence of chains, one could expect also for small k vortices an increase of the threshold Reynolds number Re_1. On the contrary, incorporating the elongational term $(\lambda_2 \neq 0)$ in the magnetization balance changes the momentum balance of the vortex flow such that the growth of vortices is enhanced for $k < k_{cross}$ (left in **Figure 10**) and reduced for $k > k_{cross}$ (right in **Figure 10**) relative to the reference case of $\lambda_2 = 0$.

4.4 Nonlinear analysis

4.4.1 Bifurcation thresholds

Following, we will consider the full nonlinear ferrohydrodynamical equation of motions incorporating elongational flow effects (11) in order to investigate the influence of a finite transport coefficient λ_2 at different applied magnetic fields.

The general modification in the bifurcation threshold of primary instabilities ((w)TVF) and ((w)SPI) due to finite values $\lambda_2 \neq 0$ remains qualitative as detected and described before in the linear stability analysis in pure axial field. However, the absolute values are slightly different. A direct comparison for axial field (**Figures 9**-**11**) results in variation about one to two percent between the calculated onsets using either the linear analysis or full nonlinear equations [6]. While the different field orientations result in different magnitudes of stabilization of the basic states CCF and 2-CCF, respectively, as discussed in Section 3.3.4, a finite value λ_2 does *not* depend on different field orientations. The variation effect with λ_2 is almost identical for all considered field configuration. However, in general, the modifications are slightly larger under oblique magnetic fields. Depending on other system parameters, e.g., wavenumber k, cylinder rotation speeds Re_1, Re_2, the effect is either stabilizing or destabilizing with respect to the situation $\lambda_2 = 0$ (**Figure 10(c)** and **Figure 11**). Considering the effect of elongational flow, the critical bifurcating point of primary centrifugal instability will be shifted either up or down. As detected in the linear analysis, the potential destabilizing effect of λ_2 *never overcomes* the general stabilizing effect of the external applied magnetic field, i.e., comparing $\lambda_2 = 0$ and any value $\lambda_2 \neq 0$.

4.4.2 Flow structure modifications

Aside the modification of the primary stability thresholds, there are further flow structural changes/modifications which can be observed for finite value λ_2. **Figure 11** shows, for different field configurations T: $(s_x = 0.1, s_z = 0)$, A: $(s_x = 0, s_z = 0.1)$, O: $(s_x = 0.1, s_z = 0.1)$, how the maxima of vorticity η vary for either the full flow structure $\Delta\eta$:=$\eta(\lambda_2 \neq 0) - \eta(\lambda_2 = 0)$ (**Figure 12(a)**), and reduced 2-fold subspace (**Figure 12(b)**) varies with λ_2 for the basic state configuration $(\mathrm{Re}_1 = 60, \mathrm{Re}_2 = 0)$. Remember, that only for $s_x = 0$, one has the classical CCF, and for any $s_x \neq 0$, a modified basic state is present [6, 9, 37] (i.e., symmetry breaking effect of transversal field). Although for a given configuration (A, T, O), the absolute maxima of these values are significantly different, and their relative differences Δ scale is *linear* with λ_2 starting at zero. Lines in **Figure 12** are calculated by linear regression fitting to the numerical data points. The effect of λ_2 is *decoupled* from the magnetic field configuration and with this the considered flow structure.

Either for classical "pure" CCF or field modified 2-CCF, the variation in $\max(\Delta\eta)$ grows linear with λ_2 (**Figure 12(a)**) (note the significant smaller amplitude in the $m = 2$ subspace). Further confirmation for this is the fact that an analog linear growth can be also found when considering other parameters, at which a supercritical flow state exists [37]. This holds for toroidally closed structures (w)TVF, as well as for helical flow states (w)SPI. Only the absolute values in $\max(\Delta\eta)$ are significant larger.

It is important to mention that the slopes in **Figure 12** (for $O(s_x = 0.1, s_z = 0.1)$) not only depend on the applied field orientation (O) but also depend on the *strength* of the applied magnetic field. With increasing the magnetic field strength s_x, s_z, the slopes become steeper. This scenario is illustrated, exemplary for 2-CCF basic state in transversal field configuration in **Figure 13**.

Moreover, similar characteristics hold for the different primary bifurcating structures. **Figure 14** elucidates this effect for the three different field configurations A, T, and O as indicated (see also **Figures 4** and **6** in [37] for another example considering a transversal magnetic field in finite system configuration). For a given field configuration, the slopes increase with λ_2, when increasing the magnetic field strength s_x. In general, slopes are smallest for transversal and largest for oblique fields, respectively. The variation in the slopes is continuous with increasing the field strength, but not linear; for larger field strength, the variation in the slopes becomes smaller.

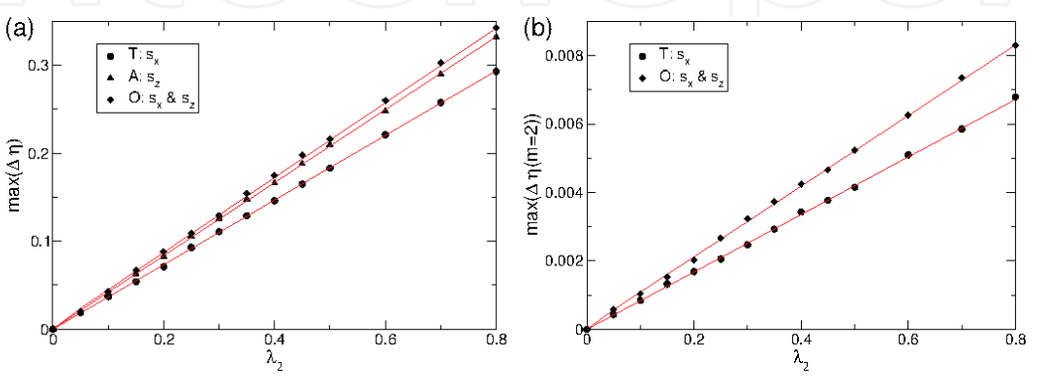

Figure 12.
Variation of vorticity maxima with λ_2 for (a) $\max(\eta) = \eta(\lambda_2) - \eta(\lambda_2 = 0)$ at full solution and (b) $\max(\eta(m = 2)) = \eta(\lambda_2) - \eta(\lambda_2 = 0)$ at only 2-fold symmetric subspace (empty for A) for basic flow (CCF and 2-CCF, respectively) at $\mathrm{Re}_1 = 60$, $\mathrm{Re}_2 = 0$ and different field orientations: Axial (A) $s_x = 0.0, s_z = 0.6$; transverse (T) $s_x = 0.6, s_z = 0.0$ and oblique (O) $s_x = 0.6, s_z = 0.6$. Lines are linear fits.

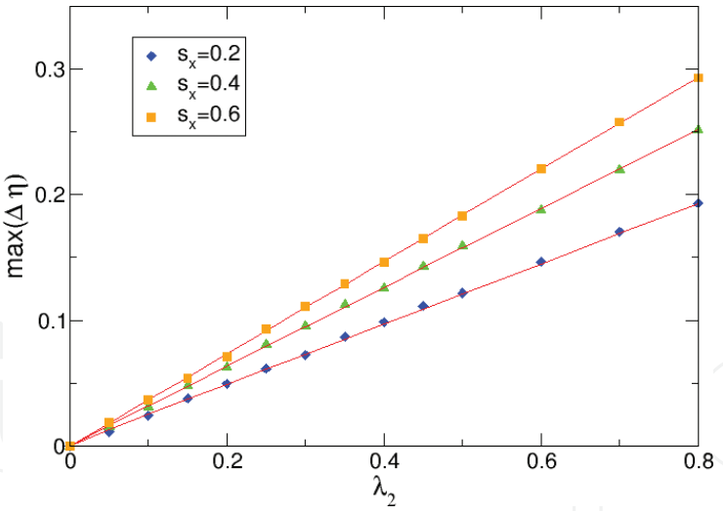

Figure 13.
*As **Figure 11** for basic state 2-CCF at* $\mathrm{Re}_1 = 60$, $\mathrm{Re}_2 = 0$. *Variation with* λ_2 *of vorticity maxima* $\max(\eta) = \eta(\lambda_2) - \eta(\lambda_2 = 0)$ *for transversal field (T) at different field strength* s_x *as indicated.*

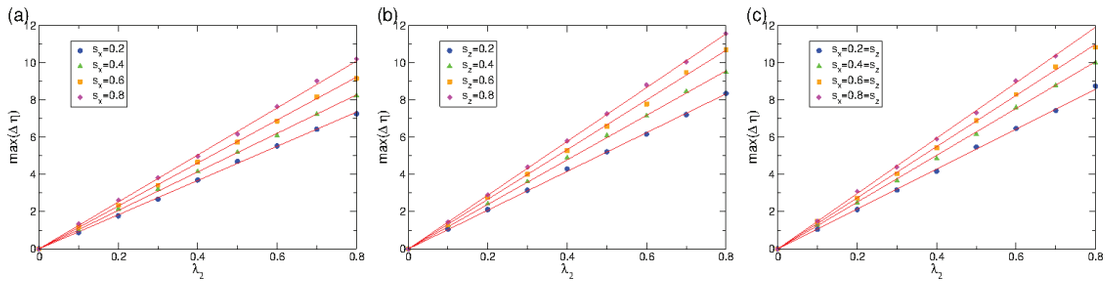

Figure 14.
Supercritical (w)TVF solution at $\mathrm{Re}_1 = 100$, $\mathrm{Re}_2 = 0$. *Variation of vorticity maxima* $\max(\eta) = \eta(\lambda_2) - \eta(\lambda_2 = 0)$ *for (a) transversal (T), (b) axial (A) and (c) oblique (O) magnetic field (strength as indicated). Lines are linear fits.*

4.4.3 Wavenumber modification and selection

As seen in the former discussion (section 4.3.2), an elongational flow can have strong effect on the axial wavenumber k. Consider the full equations (and periodic boundary conditions), one obtains similar results as presented in **Figure 10** for linear analysis of the marginal stability thresholds for TVF and SPI. As described before, the agreement between the results of linear and full equations is very close (they differ less than 2 percent).

However, in order to see such wavenumber modification from another perspective, it makes sense to study a finite system with sufficient large aspect ratio enclosed by fixed end plates (assumed to be stationary) on top and bottom. As in a finite system, the axial wavenumber k is *natural selected* by the system itself (depending on the various system parameters), it is possible to see the direct influence, considering a finite value λ_2 on to the flow structures and their axial wavenumbers k.

Starting with a classical TVF as initial flow state, with $n = 22$ vortices, which corresponds to an axial wavenumber $k = 3.41$ in the bulk (illustrated on the most left border in **Figure 15**), we consider a situation with an applied pure transversal magnetic field which is continuously increased for two values, either ignoring any elongational flow effect, $\lambda_2 = 0$ (**Figure 14(a)**), or considering such effect $\lambda_2 = 0.2$ (**Figure 15(b)**) (note 0.2 is quite small). In any case, either for $\lambda_2 = 0$ and for $\lambda_2 = 0.2$, by increasing the magnetic-field strength, s_x, the number of vortices is reduced, which leads to an increase in the axial wavelength (i.e. decrease in axial

wavenumber k) due to *elimination* of vortices in the bulk. Therefore, the corresponding axial wavenumber k in the bulk becomes reduced. Remember that the initial state is a classical, stationary TVF, which becomes modified to stationary wTVF as soon as $s_x \neq 0$. For the field generated wTVF, the wavy-like modulation is not visible in **Figure 15**. However qualitative, the same scenario also holds for either axial and oblique magnetic fields, with changes in the corresponding parameters s_x, s_z at which the wavenumber k changes, i.e., vortices disappear.

In general, the exact field strength s_x for vortex elimination and/or the number of destroyed vortices depends on λ_2. In the example of **Figure 15**, the initial flow has 22 vortices with an axial wavenumber $k = 3.41$. Neglecting elongational effects $\lambda_2 = 0$ (**Figure 15(a)**) until the parameter s_x approximately reaches the value about 0.7, the flow remains stable, and the number of vortices in the flow can be reduced to $n = 20$ with $k = 3.04$. Further increasing s_x to about 0.85, the number of vortices can be more reduced to $n = 16$ with $k = 2.58$. Hereafter, no further changes in the number of vortices n appear, before reaching the boundary threshold, $s_x \approx 0.9$. Consider elongational flow $\lambda_2 = 0.2$ (**Figure 15(b)**), the behavior of the vortex state is similar to the case neglecting such effects. The flow remains stable before the parameter s_x reaches about 0.75. At the same time, the number of vortices is also reduced in analog manner to $n = 20$ with $k = 3.04$. Hereafter, as before, the number of vortices n remains unchanged until the parameter s_x increases to the boundary threshold, $s_x \approx 0.95$. Consider values $\lambda_2 > 0.7$, the flow structure (for given parameters) is not affected by the magnetic-field strength. A flow with $n = 22$ vortices corresponding to axial wavenumber $k = 3.41$ in the bulk is remaining in the bulk.

An interesting phenomenon, which also has been reported in experimental studies [9] as in numerical simulations, is the fact that one or two vortex pairs can be eliminated. However so far, there is no physical explanation for this observation/phenomenon. Analog to the presented scenario in **Figure 15** for pure transversal magnetic field, one also finds similar reduction scenarios for pure axial and oblique magnetic fields. As to expect, the absolute values of field strength, s_x, s_z, at which the elimination of vortices happen is different, depending on the applied field.

4.5 Resume

Real ferrofluids consist of a suspension of particles with finite size and mainly almost ellipsoid shape, as well as there are particle-particle interactions that tend to

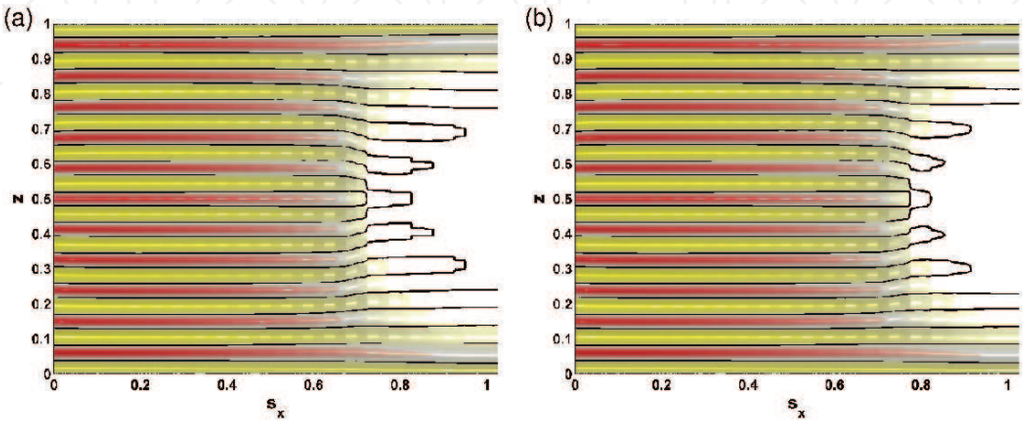

Figure 15.
Contours of the radial velocity component u at mid-gap with variation of field strength s_x at $Re_1 = 88.35$, $Re_2 = 0$ for (a) $\lambda_2 = 0$ and (b) $\lambda_2 = 0.2$. Left border in each plot gives the initial state, a classical TVF with n = 22 vortices corresponding to an axial wavenumber k = 3.41 in the bulk. Note that for $s_x = 0$, only wavy-like modified flow states exist. Red (yellow) [dark gray (light gray)] corresponds to positive (negative) values. The max (min) level is ±9.98.

form chains of various lengths and tend to agglomerate in general. One possibility in order to make a more realistic approach for ferrofluids and to come close to such a configuration in a real ferrofluids is to consider the effect of elongational flow. Such a flow becomes incorporated by the symmetric part of the velocity gradient field tensor in the nondimensional ferrohydrodynamic equations of motion (11) and scales by a material dependent transport coefficient λ_2. By such an assumption, the latter is given by a pure scalar number, describing the strength/influence of all former mentioned properties.

Consider either linear stability analysis or fully nonlinear equations, one finds that incorporating such elongational flow can have either stabilization or destabilization effect (i.e., modification in the supercritical primary bifurcation thresholds) with respect to the reference situation in absence of such flow ($\lambda_2 = 0$). The modifications due to finite value λ_2 are qualitative similar and in the same range for different considered magnetic fields, slightly largest in case of an oblique field compared to pure axial or transversal ones. Typically, the modifications due to $\lambda_2 \neq 0$ are larger for helical, nonaxisymmetric, $m = 1$, (w)SPIs than for toroidally closed, axisymmetric, $m = 0$, (w)TVF. Thus, the regim of primary stable bifurcating (w)TVF increases. This observation is similar and goes in hand with the previously described general stabilization of any applied magnetic field (Section 3). There we saw that the stability thresholds of helical flow states are shifted further than those of toroidal closed flow structures. However, it is important and fundamental to state that the elongational effect $\lambda_2 \neq 0$ is *never* big enough to *over compensate* the general, field-induced stabilization. Only the magnitude/amplitude in shift can be reduced. Further, it is worth to mention that linear stability analysis is limited to axial magnetic fields; as for fields with finite transversal component, no basic state can be derived, simulations of full nonlinear equations confirm similar effects. The modifications due to λ_2 are sensitive to various different system parameters (e.g., Reynolds numbers, radius ratio, etc.), in particular sensitive to the axial wavenumber k. Here, smaller k are strongly effected than larger ones. Thus, considering finite size TCS, a considered elongational flow results in modifications of flow structures in the sense of changing number of vortices in the bulk, which coincides with a different wavenumber selection. Thus, depending on the particular wavenumber, the presence of any elongational effect $\lambda_2 \neq 0$ can be either stabilizing or destabilizing for the basic state. In finite system, this results in different selection and/or modification of number of vortex pairs within the annulus, depending on the parameter.

Regarding the flow structural properties, a finite transport coefficient, $\lambda_2 \neq 0$, does *not* change the qualitative shape of the flow pattern. Only quantitative differences can be observed. Essentially, all structural properties remain as generated/induced due to the external applied magnetic field. Thus for instance, the azimuthal mode-2 symmetry originated in the symmetry-breaking transverse magnetic field is preserved; only the strength of different flow quantities is modified (in general they increase) according to finite λ_2. Mainly, the flow states become *linearly enforced*, e.g., speaking in quantity of the azimuthal vorticity, which holds for both the basic flow (CCF, 2-CCF) and the primary instabilities the supercritical centrifugal unstable flows ((w)TVF, (w)SPI).

5. Modified field dependence - internal magnetization

5.1 Introduction and motivation

Aside the properties and behavior of the magnetic particles itself and their interaction with the applied magnetic field (see last sections), the correct

assumption of the applied magnetic field is another crucially point in describing magnetic flows and their dynamics. The frequently used, most common assumption is to consider the internal magnetic field within the magnetic fluid (e.g., a ferrofluid) to be *equal* to the external applied field. Following, we will see that this is only a leading-order approximation. By accounting for the ferrofluid's magnetic susceptibility, a uniform externally imposed magnetic field is modified by the presence of the magnetic fluid (ferrofluid) within the annulus. The modification to the magnetic field appears in an radial dependence $1/r^2$ and their magnitude scales with the susceptibility χ. To be concrete, such modification to the imposed magnetic field can be substantial, also for ferrofluids typically used in laboratory experiments. These have significant consequences on the structural properties and stability of the basic states, as well as on the supercritical (primary) bifurcating solutions.

5.2 Modified internal magnetic field

As already seen in the previous sections, for solving the equation of motion (1), we have to consider the magnetic field within the annular gap between the cylinders. In the last sections, we used the simplest approach with the assumption to take the magnetic field to be identical to the applied external field [4, 6]. However, this simple approach is only a leading-order approximation, and depending on the magnetic susceptibility of the ferrofluid, the magnetic field in the gap is modified.

Assuming infinitely long cylinders, the magnetic boundary conditions are

$$\vec{H} = \vec{H}_{ext} - M_r \vec{e}_r \tag{14}$$

at $r = r_1$ and $r = r_2$, where $\vec{H}_{ext}$ is the homogeneous external applied magnetic field in the absence of the ferrofluid-filled annulus and M_r is the radial component of the magnetization $\vec{M}$.

The following ansatz satisfies a solenoidal field, $\nabla \cdot \vec{H} = 0$:

$$\begin{aligned} \vec{H} = \vec{H}_{ext} &+ \left[\left(a_1 - b_1/r^2\right)\cos(\theta) + \left(a_2 - b_2/r^2\right)\sin(\theta)\right]\vec{e}_r \\ &+ \left[\left(a_2 + b_2/r^2\right)\cos(\theta) - \left(a_1 - b_1/r^2\right)\sin(\theta)\right]\vec{e}_\theta \end{aligned} \tag{15}$$

and then the boundary conditions defining the external field are.

$\vec{H}(r = r_1) = \vec{H}_{ext} + \left[\left(a_1 - b_1/r_1^2\right)\cos(\theta) + \left(a_2 - b_2/r_1^2\right)\sin(\theta)\right]\vec{e}_r + \left[\left(a_2 + b_2/r_1^2\right)\cos(\theta) - \left(a_1 - b_1/r_1^2\right)\sin(\theta)\right]\vec{e}_\theta$ and $\vec{H}(r = r_2) = \vec{H}_{ext} + \left[\left(a_1 - b_1/r_2^2\right)\cos(\theta) + \left(a_2 - b_2/r_2^2\right)\sin(\theta)\right]\vec{e}_r + \left[\left(a_2 + b_2/r_2^2\right)\cos(\theta) - \left(a_1 - b_1/r_2^2\right)\sin(\theta)\right]\vec{e}_\theta$.

To calculate the four unknown constants (a_1, a_2, b_1, b_2) from the boundary conditions (12), we need the radial component of the magnetization which results from substituting (13) into the magnetization (3):

$$\begin{aligned} M_r = &\left[\chi H_{ext}^T + \chi(a_1 - b_1/r^2) - c_N\Omega(a_2 + b_2/r^2)\right]\cos(\theta) \\ &+ \left[c_N\Omega H_{ext}^T + \chi(a_2 - b_2/r^2) + c_N\Omega(a_1 + b_1/r^2)\right]\sin(\theta), \end{aligned} \tag{16}$$

where H_{ext}^T stands for the transverse component of $\vec{H}_{ext}$. Using the continuity of the magnetic field condition on the cylinders, the coefficients can be calculated. Substituting them into (13), finally the resulting magnetic field is given by

$$\vec{H} = -\left(2\mathrm{H}_{ext}^{T}/K\right)\left(r_1/r^2\right)\left\{[\chi\cos(2\theta) + \Omega c_N \sin(2\theta)]\vec{e_x} + [\chi\sin(2\theta) + \Omega c_N \cos(2\theta)]\vec{e_y}\right\}, \tag{17}$$

where $K = (2+\chi)^2 - \chi^2\eta^2$. A special case of (15) when $\Omega c_N = 0$. This corresponds to an equilibrium magnetization and has been already observed in an earlier work by Odenbach and Müller [38]. They considered the limit of an equilibrium magnetization and used a similar derivation of the modification of the magnetic field for a ferrofluid between two cylinders.

Based on (15), one can use the following magnetic field in the equation of motion:

$$\vec{H} = 2\frac{(2+\zeta)}{K}H_x\left[\left(1-\zeta/r^2\right)\cos(\theta)\vec{e_r} - \zeta/r^2\sin(\theta)\vec{e_\theta}\right] + H_z\vec{e_z} \tag{18}$$

the dimensionless scalar parameter

$$\zeta = \frac{\chi}{2+\chi}r_1^2 \tag{19}$$

characterizes the strength of the radial field dependence ζ. The ferrohydrodynamical equation of motion (6) and the Niklas parameters s_x and s_z (7) remain unchanged/untouched from such considered radial field dependence.

5.3 Flow structural modifications

5.3.1 Primary instabilities

As we learned in previous sections, a magnetic field with a finite transverse component modifies either basic state or primary bifurcating flow structures in a wavy-like manner. More details of these states have been reported in numerical simulations [6], for which a homogeneous internal magnetic field equal to the external applied one has been supposed, as well as in real experimental studies [9]. The question now is how does the former derived radial field dependence ζ affects the stability of the basic states (CCF and 2-CCF) and the characteristics of the bifurcating solutions ((w)TVF and (w)SPI).

We begin our discussion by considering a purely axial applied magnetic field (A), with fixed field strength $s_z = 0.6$, which leaves the flows, in particular its structural properties unaffected (TVF and SPI). **Figure 16** shows the influence of the radial field parameter, ζ, (17) (exemplary chosen (a) $\zeta = 0$, (b) $\zeta = 0.4$ and (c) $\zeta = 0.8$), on the bifurcation thresholds for TVF and SPI in an axial magnetic field. As in absence of any field dependence, $\zeta = 0$ (**Figure 16(a)**), the bifurcations continue being supercritical. Main effect on the bifurcation curves is that with increasing ζ, the thresholds for the onset of both TVF and SPI are shifted to higher Re_1 (**Figure 16(b,c)**). Thereby, the threshold for the toroidally closed TVF being shifted significantly further (to larger values Re_1). Note the different scaling on the abscissa in **Figure 16(c)**. Aside from the enhanced stabilization of the CCF basic state on top of the field introduced stabilization itself, one observes an important consequence to the relative shifts in the two bifurcation curves. Consequently, the bifurcation curve of TVF is shifted more than the one of SPI, the co-dimension-two point, γ, is also shifted to more positive Re_2 (c.f. **Figure 15(a,b)**). Interestingly, this is just the *opposite* way of the shift with increasing field strength s_z in a pure axial magnetic field (the same holds for s_x in transversal field), which we saw in **Figure 7**

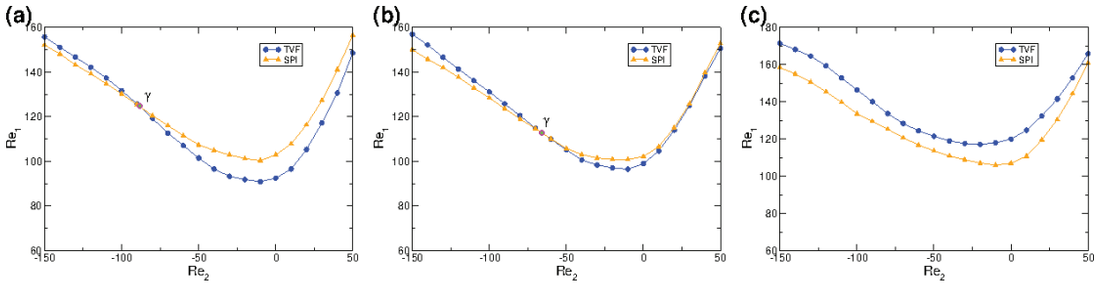

Figure 16.
Bifurcation curves for the onset of TVF (blue) and SPI (orange) in $\mathrm{Re}_2 - \mathrm{Re}_1$ *diagram for different* ζ*-values (a)* $\zeta = 0$*, (b)* $\zeta = 0.4$ *and (c)* $\zeta = 0.8$ *with an applied axial magnetic field (A) with* $s_z = 0.6$*. ((a) is a replot of* ***Figure 7(c)*** *for comparison). Note the different scale on the ordinate in (c). Simulation results of full nonlinear equations (11) consider a short periodic TCS with axial wavenumber* $k = 3.927$ *(same hold for* ***Figures 15*** *and* ***16****).*

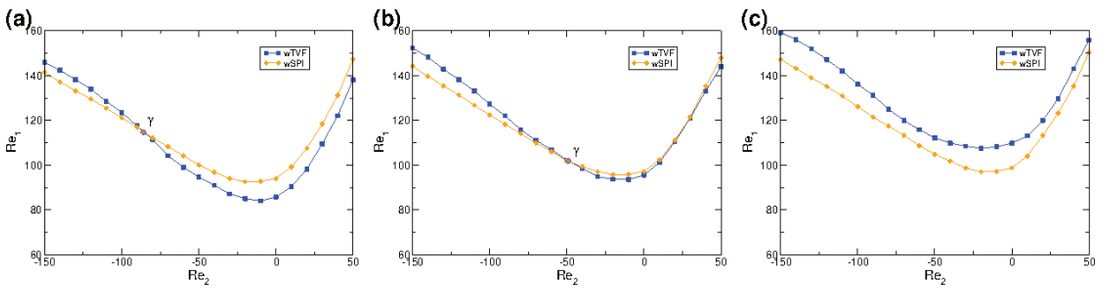

Figure 17.
Bifurcation curves for the onset of wTVF (blue) and wSPI (orange) in parameter space for different ζ *values (a)* $\zeta = 0$*, (b)* $\zeta = 0.4$*, and (c)* $\zeta = 0.8$ *with an applied transversal magnetic field (T)* $s_x = 0.6$*. ((a) is a replot of* ***Figure 7(b)*** *for comparison).*

with moving the γ-point to the left toward more negative values in Re_2. Consider larger values, e.g., $\zeta = 0.8$ (**Figure 15(c)**), one sees that the co-dimension-two γ-point is even shifted to Re_2>50 out of the considered parameter space. As a result, the primary instability is always the helical SPI, even with the two cylinders in strong co-rotation. This observation is crucially different from classical TCS, both without magnetic fields and also with assumption of an applied uniform magnetic field. Thus, the radial field dependence, induced by the susceptibility of the ferrofluid-filled annulus, is seen to cause major changes in the quantitative and qualitative characteristics of the flow instabilities.

Consider a transversal magnetic field, field strength $s_x = 0.6$ (**Figure 17**) instead of an axial one, the variation by increasing ζ remains virtually and qualitatively the same, aside that now all structures are wavy-like modulated (2-CCF, wTVF, wSPI). One finds the same preference, in the sense of stronger upshifts for toroidally closed wTVF with the same result of a shift in the γ-point to the right to larger values in Re_2. Thus also here, for sufficiently strong ζ, e.g., $\zeta = 0.8$ in **Figure 17(c)**, the helical wSPI is the primary stable bifurcating solution in all presented parameter space. Comparing both, pure axial and pure transversal field (at same field strength), the up-shift, i.e., the stabilization is slightly larger in axial fields. This holds for toroidally closed (w)TVF and helical (w)SPI solutions.

Finally, this effect is even more pronounced when an oblique magnetic field is applied as illustrated in **Figure 18** for field strength $s_x = 0.6$, $s_z = 0.6$. Note also the different scale on the ordinate in **Figure 17(c)** highlighting the stronger shifts due to such field configuration. One can speculate that this enforcement is due to the axial component of the oblique field leading to a base state with w having axial shear, and the radial field dependence ζ enhances the w component of the 2-CCF base state. The combination of the base state azimuthal shear and this axial shear

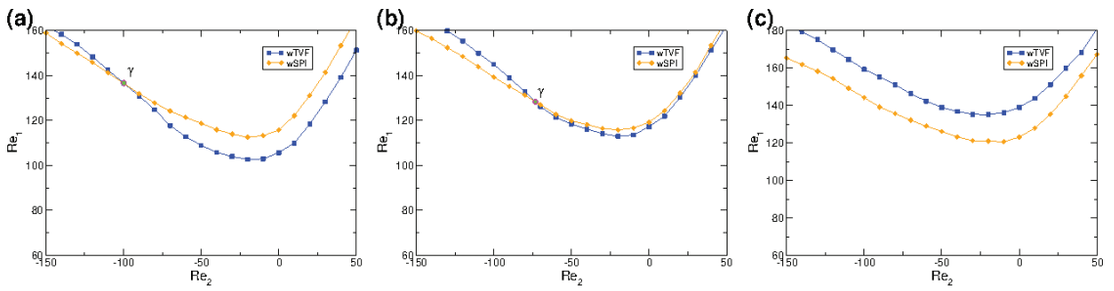

Figure 18.
Bifurcation curves for the onset of wTVF (blue) and wSPI (orange) in $\mathrm{Re}_2 - \mathrm{Re}_1$ *diagram for different* ζ*-values (a)* $\zeta = 0$*, (b)* $\zeta = 0.4$*, and (c)* $\zeta = 0.8$ *with an applied oblique magnetic field (O) with* $s_x = 0.6 = s - z$*. ((a) is a replot of* ***Figure 7(d)*** *for comparison). Note different scaling in (c).*

favors the helical instability. Close to the onset, the variation of the maxima of all flow components u, v, w is almost linear.

5.3.2 Modified flow structures

Figure 19 illustrates the flow structural properties of wTVF and wSPI in either a transverse magnetic field T (a,b) and an oblique magnetic field O (c,d), both with assumed radial field dependence $\zeta = 0.8$. Note, the flow structures of TVF and SPI under a pure axial applied magnetic field are not shown, as they virtually do not differ from the ones in absence of a magnetic field. Only the absolute values (e.g. in η) are different. Comparing these flow structures to the ones for $\zeta = 0$ cases as earlier presented in **Figure 6** (Section 3.3.3), one sees the modulations in all structures to be *enhanced/enforced*. In general, the waviness (axial variation in azimuthal direction) of

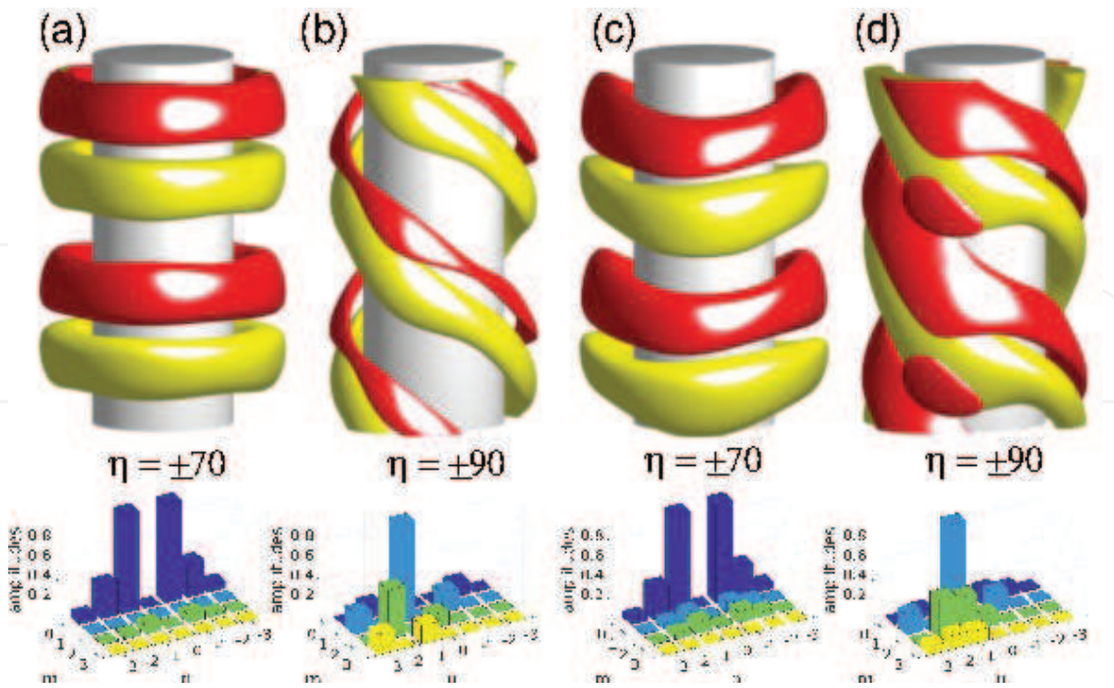

Figure 19.
(See also ***Figures 2*** *and* ***6*** *for comparison to flow states without radial field dependence. The radial field dependence is considered to be* $\zeta = 0.8$*. Top row: Azimuthal vorticity isosurfaces* η *over two axial wavelengths with pure transversal applied magnetic field (T): (a) wTVF at* $\mathrm{Re}_2 = 0$, $\mathrm{Re}_1 = -130$*, (b) wSPI at* $\mathrm{Re}_2 = -150$, $\mathrm{Re}_1 = 190$*; and with oblique applied magnetic field (O): (c) wTVF at* $\mathrm{Re}_2 = 0$, $\mathrm{Re}_1 = -150$*, and (f) wSPI at* $\mathrm{Re}_2 = -150$, $\mathrm{Re}_1 = -200$ *Red (yellow) isosurfaces correspond to positive (negative) values as indicated. The bottom row shows the mode amplitudes* $|u_{m,n}|$ *of the radial velocity field u corresponding to the structures above over the m-n-plane.*

all flow structures is enforced/enhanced by the radial dependent magnetic field. However, the field-induced wTVF always remains a *stationary*, *nonrotating,* and *phase-pinned* structure, irrespective of whether the radial field dependence is considered or not. On the other hand, wSPIs bifurcate as degenerated solutions, either as a left- or right-winding SPI, depending on initial conditions. Their corresponding frequencies remain mainly constant over a wide range and do not differ much (about 20% or less) from those of SPI. Comparing the stimulated modes for flow structures when $\zeta = 0.8$ (bottom in **Figure 19**) to those with $\zeta = 0$ (bottom in **Figure 6**), one sees general larger mode amplitudes in the additional stimulated modes for consideration of an internal field dependence ($\zeta \neq 0$). These larger amplitudes in the field induced modes are also the reason for the increase in waviness.

5.4 Resume

Applying a magnetic field across a container of ferrofluid changes the ferrofluid's susceptibility and results in modification of the magnetic field structure within the container. So far, most theories commonly neglect such modification, either for convenience or simplicity, and at the end, there is also possibility of numerical simulations in appropriate time or feasibility at all.

However, it is a matter of fact that an external applied magnetic field is modified, depending on the magnetic susceptibility. Experimental studies [10, 38] confirmed the modifications also for susceptibilities of commonly used ferrofluids. Consider such modifications to the imposed magnetic field effects the basic state, its stability, as well as the primary (supercritical) bifurcating solutions. This holds for any field configuration, with only differences in the strength of modifications, i.e., the stabilization (its magnitude; up-shift, move of the bifurcation thesholds to larger control parameters). On the other hand, the flow structural properties remain qualitative unaffected by such an radial field dependence, only change in quantitative manner. They are determined only by the general kind and orientation of the applied magnetic field. Thus, a pure axial field does not have any effect on the flow structural properties, leaving them as in absence of any field, i.e., pure TVF and pure SPI. As described before, the presence of a finite transversal field component results in a wavy-like modulated flow state. This is independent/untouched if the magnetic field is considered to be homogeneous or inhomogeneous with a radial field dependence. However, consider stronger modifications to the imposed magnetic field, i.e., larger values of the radial field dependence parameter ζ have the effect of further strengthening the already present waviness of the structures. This holds for (w)TVF and (w)SPI alike. An important observation is the different influence of the radial field dependence ($\zeta \neq 0$) onto topological closed and helical flow states. In general, the effect of modification in the primary bifurcation thresholds is larger for toroidally closed flow structures compared to helical ones. As a result, their intersection point, i.e., co-dimension γ-point is moved toward positive Re_2, which is just the opposite direction, as it moves with increasing the magnetic field strength (for any given field configuration, e.g. **Figure 7**). The parameter space, the area for which (w)SPI bifurcate primary stable out of the basic state, is growing, even into region of co-rotating cylinders, i.e. $Re_2>0$, making wSPI the favorable flow state in the system.

6. Conclusions

Although there has been significant progress in the understanding of ferrofluidic flows in the past decades, their fully theoretical understanding is still limited. A key

reason for this is computational high-expensive simulations, which even increase with continuation in refining the models to make them more realistic/appropriate, e.g., finite size effects, internal field modifications, etc. However, these model improvements are essential and necessary to uncover the full potential of ferrofluids, which already are used in a wide field of applications. The use in the car industry within antishocks to provide adjustable damper settings is probably one of the most prominent examples. However, either experiments and numerics are essential to mutually prove each other and combined to provide new inside of potential applications.

This chapter deals with a rotating ferrofluid between two concentric cylinders, i.e., ferrofluid in Taylor-Couette geometry. Therefor we consider different improvements in the model describing such magnetic particles in a flow under external applied field. Concluding the discussions, the main points can be summarized as follows:

- Any applied magnetic field changes the bifurcation thresholds of primary solutions—the thresholds of both primary solutions, TVF and SPI, are shifted to larger parameter values—the *basic state becomes stabilized* against perturbations.

- Magnetic fields with a finite transversal component break the system symmetry and renders all flow states to be *inherently 3*D. As a result, the pure flow states TVF and SPI cease to exist and are substituted by their wave-like cousins, wTVF and wSPI. Thereby, the generated wTVF differs crucially from the classical ones, which rotate in azimuthal direction. Instead, the magnetic field induced wTVFs are *nonrotational, phase-pinned* flow solutions and develop *belly shape structure* at specific azimuthal positions.

- Assuming *elongational flow*, in order to consider *finite-size effect* of the magnetic particles and their interaction (agglomeration, particle-particle interaction and chain formation procedures), one detects further changes in the bifurcation threshold of the solutions. Also, this can result in further *stabilization* or *destabilization*. However, the effect of such elongational flow is *never* big enough to over-compensate the general, field-induced stabilization. Only the magnitude/amplitude varies. The flow states remain structural as in absence of elongational flow.

- Accounting for the changes in ferroluid's susceptibility in the container due to an external magnetic field, the real internal field can be approximated by $1/r^2$. As before the flow, structural properties remain qualitative similar. Bifurcation thresholds are shifted upward, toward larger Re_1, whereby toroidally closed (w)TVFs are in general preferred and shifted more than helical (w)SPI. The result is an increase in the regime of primary bifurcating (w)SPI.

A. Appendix

A.1 Numerical method

There are various different ways to solve the ferrohydrodynamic equations of motions (Eqs. (5) and (10)), the latter including elongational flow). All here presented results have been obtained by a code (G1D3 [6, 7]), which combines a finite difference method of second order in (r,z) and time (explicit) with spectral decomposition in θ [6]:

$$f(r,\theta,z,t) = \sum_{m=-m_{max}}^{m_{max}} f_m(r,z,t)e^{ink\theta}, \tag{20}$$

where f denotes one of $\{u,v,w,p\}$. For the parameter regimes investigated here, $m_{max} = 8$ provides adequate accuracy. For discretization, a forward time, centered space (FTCS) algorithm is used on staggered grids in the $r-z$ plane following the procedure of Hirt et *al.* [45]. In particular, a homogeneous grid with discretization length $\delta_r = \delta_z = 0.05$ and time steps $\delta t < 3800$ has been used. Here, δt defines the time step between two iterations via FTCS algorithm of the system of coupled equations for the amplitudes $f_m(r,z,t)$ of the azimuthal normal modes $-m_{max} \leq m \leq m_{max}$. For diagnostic purposes, the complex mode amplitudes $f_{m,n}(r,t)$ were calculated obtained from a second axial Fourier decomposition:

$$f_m(r,z,t) = \sum_n f_{m,n}(r,t)e^{inkz}, \tag{21}$$

where $k = 2\pi/\lambda$ is the axial wavenumber.

Acknowledgments/Funding

S. Altmeyer is a Serra Húnter Fellow. This work was supported by the Spanish Government grant FIS2017–85794-P.

Conflict of interest

The author declares no conflict of interest.

Nomenclature and abbreviations

TCS	Taylor-Coutte System
NSE	Navier–Stokes equation
CCF	Circular Couette flow [basic flow]
2-CCF	2-fold CCF [basic flow in transversal field]
TVF	Taylor vortex flow
SPI	Spiral vortex flow (spiral)
wTVF	wavy TVF
wSPI	wavy SPI

IntechOpen

Author details

Sebastian Altmeyer
Castelldefels School of Telecom and Aerospace Engineering, Universitat Politècnica de Catalunya, Barcelona, Spain

*Address all correspondence to: sebastian.andreas.altmeyer@upc.edu

References

[1] Rosensweig RE. Ferrohydrodynamics. Cambridge University Press, Cambridge; 1985. 344 pp. Journal of Fluid Mechanics, 200, 597-599 DOI: 10.1017/S0022112089220773

[2] Hart JE. Dynamics of Atmospheres and Oceans. 2006;**41**. DOI: 10.1016/j.dynatmoce.2006.03.001

[3] Hart JE, Kittelman S. Dynamics of Atmospheres and Oceans. 2006; **41**:139. DOI: 10.1017/S0022112075001309

[4] Niklas M. Zeitschrift fuer Physik B: Condensed Matter. 1987;**68**:493. DOI: 10.1007/BF01471080

[5] Niklas M, Müller-Krumbhaar H, Lücke M. Journal of Magnetism and Magnetic Materials. 1989;**81**:29. DOI: 10.1016/0304-8853(89)90225-4

[6] Altmeyer S, Hoffmann C, Leschhorn A, Lücke M. Physical Review E. 2010;**82**: 016321. DOI: 10.1103/PhysRevE.82.016321

[7] Leschhorn A, Lücke M, Hoffmann C, Altmeyer S. Physical Review E. 2009;**79**: 036308. DOI: 10.1103/PhysRevE.79.036308

[8] Reindl M, Leschhorn A, Lücke M, Odenbach S. Journal of Physics: Conference Series. 2009;**149**:012109. DOI: 10.1088/1742-6596/149/1/012109

[9] Reindl M, Odenbach S. Physics of Fluids. 2011;**23**:093102. DOI: 10.1063/1.3633341

[10] Odenbach S, Müller HW. Journal of Magnetism and Magnetic Materials. 2005;**289**:242. DOI: 10.1016/j.jmmm.2004.11.069

[11] Mahle S, Ilg P, Liu M. Physical Review E. 2008;**77**:016305. DOI: 10.1103/PhysRevE.77.016305

[12] Müller HW, Liu M. Physical Review E. 2001;**64**:061405. DOI: 10.1103/PhysRevE.64.061405

[13] Debye PJW. Polar Molecules. New York: Dover; 1929 https://hdl.handle.net/2027/uc1.$b45989

[14] McTague JP. The Journal of Chemical Physics. 1969;**51**:133. DOI: 10.1063/1.1671697

[15] Martsenyuk MA, Raikher YL, Shliomis MI. Soviet Physics - JETP. 1974;**38**:413 http://www.jetp.ac.ru/cgi-bin/dn/e_038_02_0413.pdf

[16] Gilles de GP, Prost J, editors. The Physics of Liquid Crystals. Oxford: Clarendon; 1983. ISBN: 9780198517856

[17] Leschhorn A, Embs JP, Lücke M. Journal of Physics: Condensed Matter. 2006;**18**:S2633. DOI: 10.1088/0953-8984/18/38/S07

[18] Embs JP, May S, Wagner C, Kityk AV, Leschhorn A, Lücke M. Physical Review E. 2006;**73**:036302. DOI: 10.1103/PhysRevE.73.036302

[19] Taylor GI. Philosophical Transactions of the Royal Society of London A. 1923;**223**:289. DOI: 10.1098/rsta.1923.0008

[20] Chossat P, Iooss G. The Couette-Taylor Problem. Berlin: Springer; 1994. DOI: 10.1007/978-1-4612-4300-7

[21] Langevin P. Annales de Chimie Physique. 1905;**5**(70)

[22] Embs J, Müller HW, Wagner C, Knorr K, Lücke M. Physical Review E. 2000;**61**:R2196. DOI: 10.1103/PhysRevE.61.R2196

[23] Odenbach S, Gilly H. Journal of Magnetism and Magnetic Materials.

1995;**152**(123). DOI: 10.1016/0304-8853(95)00442-4

[24] Altmeyer S, Lopez JM, Do Y. Physical Review E. 2012;**85**:066314. DOI: 10.1103/PhysRevE.85.066314

[25] Zubarev AY, Skakova Y. Physical Review E. 2000;**61**:5415. DOI: 10.1103/PhysRevE.61.5415

[26] Golubitsky M, Stewart I, Schaeffer D. Singularities and Groups in Bifurcation Theory II. New York: Springer; 1988. ISBN: 978-1-4612-4574-2

[27] Golubitsky M, Stewart I. SIAM Journal on Mathematical Analysis. 1986; **17**:249. DOI: 10.1137/0517023

[28] Ch H, Altmeyer S, Pinter A, Lücke M. New Journal of Physics. 2009;**11**: 053002. DOI: 10.1088/1367-2630/11/5/053002

[29] Davey A, Di Prima RC, Stuart JT. Journal of Fluid Mechanics. 1968;**31**:17. DOI: 10.1017/S0022112068000029

[30] Iooss G. Journal of Fluid Mechanics. 1986;**173**:273. DOI: 10.1017/S0022112086001179

[31] Altmeyer S, Do Y, Marques F, Lopez JM. Physical Review E. 2012;**86**:046316. DOI: 10.1103/PhysRevE.86.046316

[32] Coles D. Journal of Fluid Mechanics. 1965;**21**:385. DOI: 10.1017/S0022112065000241

[33] Wereley ST, Lueptow RM. Journal of Fluid Mechanics. 1998;**364**:59. DOI: 10.1017/S0022112098008969

[34] Jones CA. Journal of Fluid Mechanics. 1981;**102**:249. DOI: 10.1017/S0022112081002620

[35] Akonur A, Lueptow RM. Physics of Fluids. 2003;**15**:947. DOI: 10.1063/1.1556615

[36] King GP, Li Y, Lee W, Swinney HL, Marcus PS. Journal of Fluid Mechanics. 1984;**141**:365. DOI: 10.1017/S0022112084000896

[37] Altmeyer S, Lopez JM, Do Y. Physical Review E. 2013;**88**:013003. DOI: 10.1103/PhysRevE.88.013003

[38] Odenbach S, Müller HW. Physical Review Letters. 2002;**89**:037202. DOI: 10.1103/PhysRevLett.89.037202

[39] Müller HW, Hahn D, Liu M. Journal of Physics: Condensed Matter. 2006;**18**: S2623. DOI: 10.1088/0953-8984/18/38/S06

[40] Chang MH, Chen CK, Weng HC. International Journal of Engineering Science. 2003;**41**:103. DOI: 10.1016/S0020-7225(02)00183-0

[41] Singh J, Bajaj R. Journal of Magnetism and Magnetic Materials. 2005;**294**:53. DOI: 10.1016/j.jmmm.2004.10.123

[42] Singh J, Bajaj R. International Journal of Mathematics and Mathematical Sciences. 2005;**3727**. DOI: 10.1155/IJMMS.2005.3727

[43] Altmeyer S, Leschhorn A, Ch H, Lücke M. Physical Review E. 2013;**87**: 053010. DOI: 10.1103/PhysRevE.87.053010

[44] Reindl M, Odenbach S. Experiments in Fluids. 2010;**50**:375. DOI: 10.1007/s00348-010-0940-y

[45] Hirt CW, Nichols BD, Romero NC. NASA STI/Recon Technical Report N; 1975. http://adsabs.harvard.edu/abs/1975STIN...7532418H